Transport Properties of Helium near the Liquid–Vapor Critical Point. IV. The Shear Viscosity of ³He and ⁴He

Charles C. Agosta,* Suwen Wang, L. H. Cohen,† and H. Meyer

Department of Physics, Duke University, Durham, North Carolina

Shear viscosity measurements with a precision of 0.05% are reported for ³He and ⁴He along near-critical isochores $0.85 < \rho/\rho_c < 1.12$, where ρ_c is the critical density. The temperature range was $-10^{-4} < \varepsilon < 1$, where $\varepsilon = (T - T_c)/T_c$ is the reduced temperature. The experiments were carried out with a torsional oscillator operating at 158 Hz, driven at resonance in a phase-locked loop. The absolute value of the viscosity was obtained by calibration at the superfluid transition of ⁴He, based on published values and from direct calculations using the free decay time constant of the oscillations. The data are analyzed in terms of a model using the recent mode-coupling (MC) expressions by Olchowy and Sengers, and where account is taken of the earth's gravity effects. The theory could be fitted very well to the experiment with a single free parameter, the cutoff wave number q_D, which was found to be 3.0×10^6 and 7.0×10^6 cm^{-1} for ³He and ⁴He, respectively. We have used for the critical exponent the MC predicted value of $z_\eta = 0.054$, which permits a fit superior to that using $z_\eta = 0.064$ predicted by dynamic renormalization group (DRG) theories. Detailed comparisons are made between the model calculations and data for various isochores and isotherms and good agreement is obtained. The effects of gravity are described in some detail. The predicted frequency effect in viscosity measurements is calculated for ³He and is shown to be obscured by gravity effects. Using the Olchowy–Sengers formulas, we have also fitted the MC theory to the critical thermal conductivity data of ³He, again with q_D as the only free parameter. This fit gave $q_D = 6 \times 10^7$ cm^{-1}, which in the ideal situation should have been the same as q_D from viscosity. We also discuss a representation of the ³He viscosity data along the critical isochore by a power law and first correction-to-scaling term. Using the viscosity and the critical conductivity data for ³He, we have calculated the dynamic amplitude ratio and obtained $\mathcal{R} = 1.05 \pm 0.10$, in agreement with predictions from MC and DRG theories. Also, $\mathcal{R}$ agrees with data of classical fluids. Finally, a comparison is made of recent shear viscosity data for CO_2 by Bruschi and Torzo with those on He. The CO_2

---

*Present address: Department of Physics, Harvard University, Cambridge, Massachusetts.
†Present address; Bell Laboratories of AT&T, Middletown, New Jersey.

data are also analyzed in terms of the MC theory, and the discrepancies are discussed. In the Appendices, we present the results of new compressibility measurements on ^{3}He along the critical isochore, as used in the MC analysis. We also present a brief analysis of the fluid hydrodynamics in the torsional oscillator leading to relations for the viscosity as a function of the measured quantities. Finally, we give a short outline of the vertical density profile calculations from the earth's gravity field for the calculations of the viscosity near T_c.

1. INTRODUCTION

The shear viscosity η near critical points has been of interest for a number of years, and the modern statistical techniques have dealt with this property at quite some length.[1-3] Although abundant viscosity data exist for mixtures near consolute points[1,4,5] and for pure classical fluids[1,6,7] near the liquid–vapor critical point T_c, no viscosity results have been reported for ^{3}He and only preliminary ones for ^{4}He near T_c.[8] Because of the availability of other transport and static properties data for ^{3}He,[9-12] a systematic study of the shear viscosity along several near-critical isochores seemed an obvious extension of the program carried on in this laboratory for a number of years. In this paper we report measurements of η in ^{3}He and ^{4}He using a torsional oscillator operating at 158 Hz. A wide temperature range is covered to permit the determination of the singular behavior of η above T_c and also of the regular (or background) value of the η at several densities. We take advantage of a recent improvement in the mode-coupling (MC) formulation by Olchowy and Sengers[13] to fit their theory to the experiments. Special attention is paid to the gravity effects (which are particularly severe for helium) and also to the predicted frequency effects.[14] We also discuss the differences in the background viscosity behavior between ^{3}He and ^{4}He.

In Section 2, a brief review is given of recent theoretical progress on the critical shear viscosity. Section 3 is concerned with a description of the viscometer operation principles and its construction, and with other experimental techniques. In Section 4, the experimental procedures are described and also calculations pertinent to the viscometer, such as shear stress. Model calculations for the measured apparent viscosity as affected by gravity are described in Section 5, and in Section 6 the experimental results are presented and analyzed with the help of predictions. The conclusions are summarized in Section 7. In Appendix A we quote the MC expressions used to fit the theory to both shear viscosity and thermal conductivity data. In Appendix B, new compressibility data for ^{3}He along the critical isochore are reported. In Appendix C the relevant equations for the torsional oscillator are presented. Appendix D contains a brief outline of the cubic model formulas used for the gravity effects calculation.

2. DYNAMIC THEORY REVIEW

At the present time, static critical properties for magnets and fluids near critical points appear to be well described by renormalization group (RG) theories, not only in the asymptotic regime close to T_c, but also in the regime where "corrections to scaling" become important.[15] For binary mixtures near the consolute point—and hence for pure fluids near T_c—expressions from the dynamic renormalization group (DRG) theory with corrections-to-scaling terms have been developed very recently.[4] However, there has not yet been a derivation of crossover functions, spanning the temperature range between the background and the asymptotic critical behavior, as there has been for transport near the superfluid transition in ^{4}He.[16,17] Another theoretical approach, the mode coupling theory (MC),[2] has been developed[13,18] to the point where it includes not only the asymptotic critical, but also the crossover region into the background regime. In the analysis of our transport property data, we shall use the improved solutions to the MC equations recently developed by Olchowy and Sengers,[13] which are quoted in Appendix A. Since the completion of this analysis, Olchowy and Sengers have made further refinements to their expressions. However, these authors believe[13] that the numerical differences in the data analysis between these sets of calculation should be negligible. We shall also compare our data with the correction-to-scaling expressions presented by Beysens et al.[4]

2.1. Olchowy–Sengers Formulation

The two properties of interest here are the shear viscosity η and the thermal conductivity λ, assumed to be the sum of a regular (or background) part $\bar{\lambda}$ and a singular part $\Delta\lambda$,

$$\lambda = \bar{\lambda} + \Delta\lambda, \qquad \eta = \bar{\eta} + \Delta\eta \tag{1}$$

The conductivity is related to the thermal diffusivity $D_T = \lambda/\rho C_p$, where ρ is the mass density and C_p the specific heat per unit mass, and in turn D_T is related to the decay rate of the fluctuations $\Gamma = D_T q^2$, where q is the wave number of the order parameter fluctuations. This decay rate is also expressed by a "background" and a singular term

$$\Gamma = \bar{\Gamma} + \Delta\Gamma = \frac{\bar{\lambda} q^2}{\rho C_p(q)} + \frac{\Delta\lambda}{\rho C_p(q)} q^2 \tag{2}$$

Here we note that the background term $\bar{\Gamma}$ is not constant, because C_p diverges strongly and can be approximated by a power law. (However, $\bar{\lambda}$ has only a mild temperature dependence.) Also, we note that an explicit q dependence of C_p has been assumed that is treated in the Ornstein–Zernike approximation.[13]

In the mode-coupling approach to the critical transport problem, energy transfer between heat currents and density currents is examined with the order parameter fluctuations acting as a coupling between these modes. According to Kawasaki,[2] it is the increasing fluctuation amplitude of the density (the order parameter) and its lengthening decay times that will increase the lifetime of the intermediate states where thermal and viscous modes are excited during fluctuations, and which in turn lead to an increase in the microscopic transport coefficients.

The critical viscosity and conductivity are obtained starting from two coupled integrals that are derived from the Langevin equations of motion.[2] Of these equations, one is for the critical relaxation rate Γ, which slows down as T_c is approached, giving $\Delta\lambda$, and the second one is for the diverging viscosity.

For the viscosity, Olchowy and Sengers obtained a solution of the form

$$\eta = \bar{\eta} e^{-(z_\eta H)} \tag{3}$$

where $H = H(q_D\xi, F/G, B)$ is a lengthy function quoted in Appendix A, and where*

$$B = \rho C_v(0)/A\rho^2\beta_T(0)$$

$$G = \bar{\sigma}\rho k_B T/6\pi\bar{\eta}^2\xi \tag{4}$$

$$F = \bar{\lambda}/\bar{\eta}A\rho^2\beta_T(0)$$

$$A = (T/\rho^2)(\partial P/\partial T)_\rho$$

Here $\beta_T(0)$ is the static compressibility and P the pressure, which are measured as a function of the reduced temperature $\varepsilon \equiv (T - T_c)/T_c$. Also, $\bar{\sigma} = 3\pi/8$ is the limiting value for $q\xi \to \infty$ of a function introduced by Ferrell,[19] $\sigma(q, \xi)$. Furthermore, ξ is the correlation length $\xi = \xi_0\varepsilon^{-\nu}$ along the critical isochore with $\nu = 0.63$, and the exponent z_η is given by

$$z_\eta = 8/(15\pi^2) = 0.054 \tag{5}$$

With the exception of q_D, the cutoff wave number, all the parameters listed in Eqs. (3) and (5) are known from experiments. Hence, in principle, expression (3) can be fitted to the experiments near T_c with one single free parameter q_D as long as the dependence of the correlation length on ε and on ρ is known. For ξ, we shall use the cubic model approximation[20,21] as will be described in Section 5 and Appendix D. Ideally, q_D^{-1} represents the smallest critical wavelength disturbance or mode that could exist in the fluid. We would expect q_D^{-1} to be of the order of the average atomic spacing in the fluid. (Fluctuations at smaller wavelengths do exist, but they contribute

*In Ref. 13, y_α and y_β correspond to G and F in Eq. (4).

to the background transport properties as predicted by kinetic theory, and not to the critical enhancement).

In the limit where $q_D\xi \gg 1$, expression (3) asymptotically reduces to the power law form[18]

$$\eta / \bar{\eta} = (Q\xi)^{z_\eta} \tag{6}$$

where Q is a function of the various quantities listed in Eq. (4) and is a weak function of ε. The nonconstancy of Q is caused by the fact that experimentally the critical exponent γ for the compressibility does not equal 2ν.

Numerical calculations, using the complete function H in Eqs. (3) and (A.1), and inserting data for ^{3}He, show that in the asymptotic regime one still obtains a power law

$$\eta / \bar{\eta} = A\xi^{z_\eta(\text{eff})} \tag{7}$$

where A is a constant and $z_\eta(\text{eff})$ is an effective exponent that is slightly ($\sim 5\%$) lower than z_η, as will be discussed in Section 5.

There is some controversy in the predictions for the value of z_η. In the MC theory, one obtains $z_\eta = 0.054$,[18] while from DRG, the published estimates are $z_\eta = 0.065$[22,23] and $z_\eta \approx 0.054$.[24]

2.2. Corrections-to-Scaling Expressions

Beysens et al.[4] have presented expressions for the viscosity, from both the DRG and the MC approaches, that give the asymptotic terms and the first correction-to-scaling terms.

For the MC theory, they obtained

$$\eta = \bar{\eta}(Q\xi)^{z_\eta}(1 + \tilde{a}\xi^{-1} + \cdots) \tag{8}$$

where $\tilde{a}_\eta$ is a constant. This expansion is valid for $q_D\xi > 1$, a requirement that is met in helium for $\varepsilon \lesssim 5 \times 10^{-3}$, as numerical calculations show.

For the DRG approach, the result for η has almost the same form as Eq. (8). Here $z_\eta = 0.065$ from an epsilon expansion and the amplitudes corresponding to Q and $\tilde{a}_\eta$ are not specified. The correction-to-scaling term ξ^{-1} is replaced by $\xi^{-\omega_{\text{eff}}}$ with $\omega_{\text{eff}} \approx 1.1$. Expressed in terms of the reduced temperature along the critical isochore, the equation becomes

$$\eta = \bar{\eta}\varepsilon^{-y_\eta}(1 + a_\eta \varepsilon^{\bar{\Delta}} + \cdots) \tag{9}$$

with $y_\eta = z_\eta \nu$ and $\bar{\Delta} = \omega_{\text{eff}}\nu$. For all the binary mixtures except a single one that were investigated,[4] a fit of the data gave an average value $y_\eta \simeq 0.042$, corresponding to $z_\eta = 0.065$, close to the DRG prediction. For the last mixture, however, the authors[4] obtained $y_\eta = 0.031$, corresponding to a z_η even smaller than predicted by MC. The correction-to-scaling exponent was found to be $\bar{\Delta} \sim 0.7 \pm 0.4$, which is consistent with the predictions from both

MC and DRG.[4] The data analysis on the mixtures in Ref. 4 has been criticized by Sengers.[1]

2.3. The Frequency Effect in Viscosity Measurements

Parallel to the development of the MC theory, Ferrell and his collaborators[14,25] have developed a variation of this theory that they term "decoupled mode" theory. In general, the results of this theory for the viscosity divergence are similar to those we have quoted above. However, Ferrell's method brought to light an explicit frequency dependence of the viscosity, the consequence of which is that the viscosity divergence becomes blunted as T_c is approached. The cause of the phenomenon is rooted in the relationship between the perturbating (imposed) rate ω at which η is measured, and the average relaxation rate[26] $\bar{\Gamma}$ of the density fluctuations in the fluid. Essentially it is shown that if $\omega \gtrsim \bar{\Gamma}$, the fluid will not be able to follow the controlled excitations (in our case the wall motions of the torsional oscillator) and the viscosity will tend to a constant value as T_c is approached.

The actual calculation[14] of this effect is, like the MC theory, mathematically involved and furthermore cannot be put in closed form in three dimensions (3D). However, the viscosity can be conveniently extracted from calculations done in 2D and 4D. For a good approximation, one can use the results of the 2D calculation, which the authors claim is very close to the 3D case.

The frequency effect is seen as a multiplicative factor of the zero-frequency divergence, namely

$$\eta(\Omega, \xi)/\bar{\eta} = \exp\{z_\eta[H + H^1(\Omega)]\} \tag{10}$$

where H is as previously defined [Eq. (13)], $\Omega \equiv \omega/\bar{\Gamma}, \bar{\Gamma}$ can be approximated by

$$\bar{\Gamma} = k_B T/(3\pi\eta\xi^3) \tag{11}$$

and

$$H^1(\Omega) = \tfrac{1}{3}\{\text{Re}[\ln S(\Omega)] + \text{Im}[\ln S(\Omega)]\} \tag{12}$$

In this approximation, expressions for the terms in (12) are obtained as a function of Ω and are given by Eqs. (5.1) and (5.2) of Ref. 14. These allow us to make a numerical calculation of $\eta/\bar{\eta}$ versus reduced temperature for experiments done at constant frequency and density. These calculations are presented in Section 5.

2.4. The Critical Thermal Conductivity

The relaxation rate integral[2] alluded to briefly in Section 2.1 can be solved in a similar manner to that used for the viscosity, and the result[13] can be expressed by the relation

$$\Delta\lambda = (k_B T/6\pi\eta\xi)\rho C_p \Omega(q_D\xi, B) \tag{13}$$

where $\Omega(q_D\xi, B)$ is a complicated function reproduced in Appendix A, and where the symbols are the same as before. We note here that this function becomes unity in the asymptotic limit $q_D\xi \to \infty$, where $\Delta\lambda$ is represented by a simple power law, which was first derived by Arcovito et al.[27] Hence, the function $\Omega(q_D\xi, B)$ expresses a crossover correction that becomes important as ε increases. The value of q_D does not enter into the asymptotic power law expression, contrary to the situation for the viscosity [see Eq. (15)]. Therefore, we might guess that the viscosity data offer a more sensitive test to a fit with a free q_D parameter than do the conductivity data.

The dynamic amplitude ratio $\mathcal{R}$, to be discussed in Section 2.5, is incorporated into the function $\Omega(q_D\xi, B)$, with a value of $\mathcal{R} = 1.03$ assumed in the numerical calculation.

2.5. The Dynamic Amplitude Ratio $\mathcal{R}$

Sengers[1] and Beysens et al.[4] have discussed the theoretical and experimental determinations of the universal amplitude ratio $\mathcal{R}$, where

$$\mathcal{R} = \frac{\Delta\lambda}{\rho C_p} \frac{6\pi\eta\xi}{k_B T} \tag{14}$$

The early DRG predictions gave the asymptotic value for $\mathcal{R}$ as 1.2 when $q\xi \gg 1$, but the more recent results by Paladin and Peliti[23] give $\mathcal{R} \simeq 1.04$. Beysens et al.[4] estimate that higher corrections to the calculation will place the asymptotic value of $\mathcal{R}$ in the range 1.0–1.12. This result is consistent with the most recent predictions by the MC theory,[28] namely $\mathcal{R} = 1.03$. Furthermore, Beysens et al.[4] point out that, according to the DRG theory, the ratio $\mathcal{R}$ has correction-to-scaling terms similar to those in Eq. (8). Hence, one can expect a variation of $\mathcal{R}$ with ξ (or ε) that approaches an asymptotic value close enough to T_c.

In pure classical fluids near the liquid–vapor critical point and in binary mixtures, the singular thermal diffusivity $\Delta\Gamma/q^2 = \Delta\lambda/\rho C_p$ usually has been obtained from light scattering experiments and the evidence suggests that $\mathcal{R} \simeq 1.05 \pm 0.1$ from an average of the values over a number of fluids.[1,4] In the case of ^{3}He, both separate determinations of ρC_p and of $\Delta\lambda$, as well as diffusivity measurements $(\lambda/\rho C_p)$ from light scattering,[29] are available. The new measurements of η in ^{3}He permit us to test for this fluid the DRG and MC predictions for $\mathcal{R}$. This will be reported in Section 6.6.

3. EXPERIMENTAL

In this section we describe the apparatus, centered around the torsional oscillator, and the procedure to measure the viscosity. After a general introductory description of the cryostat, we deal with the oscillator itself, but relegate to Appendix D the derivation of the oscillator dynamical equations that lead to the viscosity determination. We then describe the mechanical construction and the electronics for the oscillator operation. This is followed by a description of auxiliary parts in the apparatus.

3.1. General Description

The cryostat for this experiment was designed and constructed with two special considerations in mind. First, a rigid platform at helium temperatures was needed that did not generate lateral or torsional motions of the viscometer or absorb energy from the oscillations. Second, the oscillator was to have only a weak mechanical coupling to the platform, to prevent transmission of outside vibrations. To these ends, a stiff main section was constructed that included vertical tubing, a vacuum chamber, and a platform holding a ^{4}He pot for temperature control above 1.5 K. From the platform a cradle hangs by a beryllium–copper fiber (0.3 cm diameter, 2.5 cm length), and contains the various devices (viscometer, density cell, etc.) necessary to the experiment. A 1-kg copper counterweight is rigidly connected to the cradle, giving it a torsional frequency of about 8 Hz. The fiber acts as a low-pass filter and strongly attenuates vibrations from the cryostat suspension as they propagate toward the cradle. Hence, an environment suitable for the viscometer operation at $\sim$150 Hz is established. To improve the heat transfer between platform and cradle, a copper braid is added as a heat leak. A general schematic presentation of the vacuum chamber is shown in Fig. 1. This chamber is rigidly suspended by three 2.5-cm-diameter stainless steel tubes with stiff, 1-mm-thick copper plates soldered at 12 cm intervals along their length. Two of the tubes are used as conduits for 30 single electric leads, 15 coaxial cables, and 3 sample capillaries into the cryostat. The cables and leads run from room-temperature connectors to heat sinks mounted on the underside of the vacuum chamber top plate. The third tube is used for pumping the ^{4}He from the pot, which is also provided with a continuous-fill capillary from the main ^{4}He bath. In addition, a cold-valve permits rapid filling of the pot.

The cradle itself is split into three levels by circular thick copper slabs, into which the various components could be screwed. Curved, detachable copper plates form a sheath around the cradle. The viscometer and density cell are hung from the bottom of the slabs, while various other components, such as Ge resistor thermometers, standard resistors, heaters, and a vapor
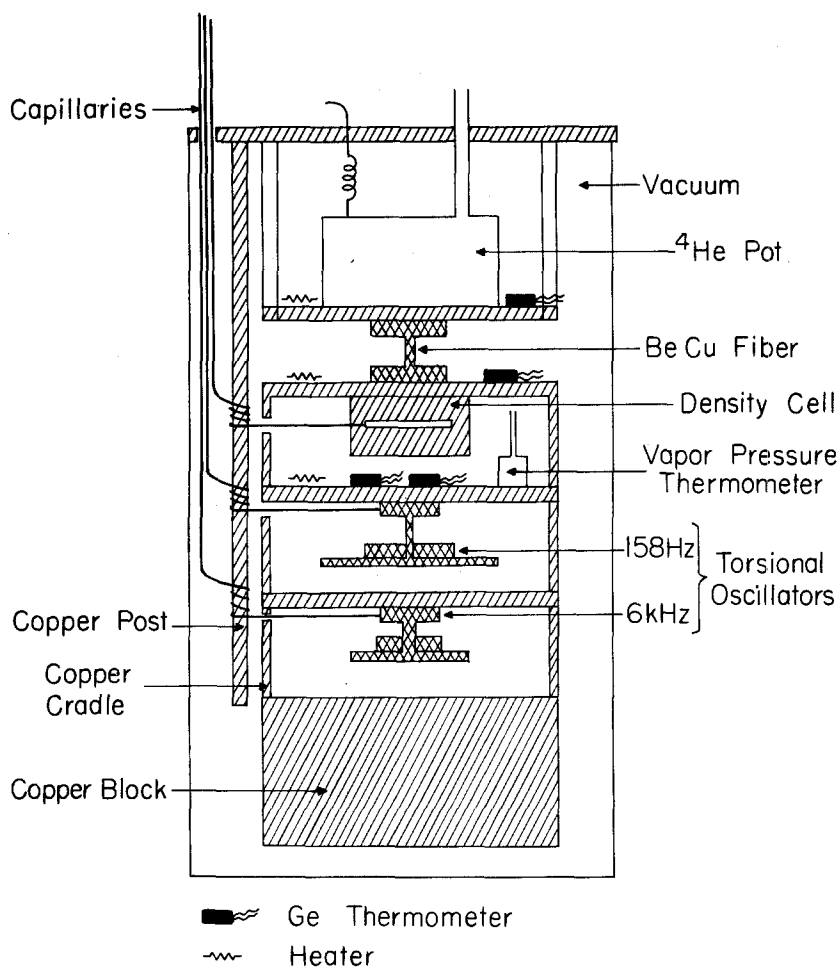
Fig. 1. Schematic diagram of the cryostat showing the vacuum chamber with the vibration isolated cradle.

pressure bulb, are attached on top of the slabs. The top level holds the density cell and the middle level supports the 158-Hz viscometer. We also experimented with a viscometer operating at 6 kHz, which was attached at the lowest level. Unfortunately, this latter device was very sensitive to vibrations in that frequency range and was not used for the measurements to be reported.

A 0.5-cm-diameter OFHC vertical copper rod soldered to the top of the vacuum chamber and extending to the copper counterweight hangs through special slots to prevent it from touching the cradle. Its purpose is

to heat-sink the capillaries to 4.2 K between the room-temperature top plate and the temperature-controlled cells, and to prevent significant amount of sample above the heat-sink location. The capillaries are made of several sections with progressively decreasing diameter as the temperature decreases. We estimate that none of the capillaries contains a mole fraction of more than 0.5% of the total sample of either cell.

3.2. The Viscometer. Design Considerations

The torsional oscillator design is based on the same principles as in the work of previous authors.[30-33] Because of certain differences in experimental conditions, it is useful to present here the relevant relations needed to derive the viscosity from the measured parameters. The details of the derivation, which starts from the Navier–Stokes equation, are given in Appendix D.

In the oscillator chamber, the fluid is contained between two horizontal circular plates of radius R spaced by a distance h, where $R \gg h$. The fluid has a viscosity η and a mass density ρ, and the disks oscillate at an angular frequency ω with an amplitude $\theta(t) = \theta_0 \sin \omega t$.

The differential equation for such a driven torsional oscillator is written as

$$I_s \ddot{\theta}(t) = -K\theta + \Gamma_D + \Gamma_f + \Gamma_E \tag{15}$$

where I_s is the moment of inertia of the empty oscillator. Furthermore, K is the elastic constant for the torsion bar,

$$\Gamma_D = D e^{-i\omega t} e^{i\Phi} \tag{16}$$

is the driving torque, and

$$\Gamma_E = \omega E \dot{\theta}(t) \tag{17}$$

is the empty-cell damping term. Finally,

$$\Gamma_f = 2 I_f \omega (i - 1) \dot{\theta}(t) \tag{18}$$

is the damping term imparted by the fluid layer on both the two horizontal walls and the vertical one of the viscometer, where

$$I_f = \tfrac{1}{4} \pi \rho \delta R^3 (R + 2h) \tag{19}$$

which is the moment of inertia of a layer of fluid one-half a penetration depth δ, with

$$\delta = (2\eta / \rho \omega)^{1/2} \tag{20}$$

The term $2h$ is the contribution of the vertical wall of height h. It is useful here to estimate the penetration depth. Using $\omega/2\pi = 158$ Hz, $\rho = 0.04$ g/cm^3 for ^{3}He near T_c, and $\eta \simeq 16 \mu$P, we obtain $\delta \simeq 9 \times 10^{-4}$ cm.

The quality factor Q_T for the total system is given by

$$Q_T = \frac{\frac{1}{2}K\theta_0^2}{\frac{1}{2}\omega^2\theta_0^2(I_f + E)} = \frac{K}{\omega^2(I_f + E)} \qquad (21)$$

For a lightly damped oscillator operating at resonance frequency $\omega_r = (K/I_s)^{1/2}$, with $Q \gg 1$ (or equivalently $I \gg I_f + E$), we have

$$Q_T^{-1} = Q_F^{-1} + Q_E^{-1} \qquad (22)$$

with

$$Q_F^{-1} \equiv I_f/I_s, \qquad Q_E^{-1} \equiv E/I_s$$

When the oscillator is at resonance, $\omega = \omega_r$, the solution of Eq. (15) for the oscillator motion finally leads to

$$D/\theta_0 = \omega_r^2(I_f + E) = K/Q_T \qquad (23)$$

The amplitude D is proportional to the driving voltage V_D applied to the oscillator, while θ_0 is proportional to the ac voltage V_{det} detected by an electronic device measuring the oscillation amplitude. Hence, one finally obtains [see Eq. (29) below]

$$V_D/V_{det} \propto Q_T^{-1} \qquad (24)$$

where the proportionality constant is a geometrical factor that can best be determined by calibration.

When the damped oscillator is not driven, but decays freely, the solution of the oscillator equation leads to an amplitude proportional to $e^{-t/\tau}$, with

$$\tau = 2Q_T/\omega_r \qquad (25)$$

The most direct way to determine Q_T is then to measure τ. This method, although time-consuming, is simple and is used to calibrate the proportionality factor in Eq. (24) for the driven oscillator mode, which is hence the most convenient and precise way to determine the shear viscosity.

In practice, the procedure is first to measure Q_E for the empty oscillator before introducing the fluid, which leads to a value for Q_F via Eq. (22). Finally, one obtains

$$\rho\eta = \frac{\omega_r}{2}\left[\frac{4Q_F^{-1}I_s}{\pi R^3(R + 2h)}\right]^2 \qquad (26)$$

We note that it is always the product $\eta\rho$ that is measured. This point has to be borne in mind when vertical density distributions in the viscometer,

due to gravity, have to be taken into account near the liquid–vapor critical point. For the optimum design that gives the highest precision in ($\eta\rho$), we need (a) to make Q_T as large as possible and (b) $Q_E \gg Q_T$. The first condition requires a very careful design to avoid losses, while for the second, a low-frequency ω_r that maximizes the ratio I_f/I_s is desirable. This ratio will be much smaller than unity anyway, as can be calculated from a reasonable choice of geometrical parameters and the known properties of the fluid. As a result, if Q_E is of the order of 10^5, Q_T will still be much larger than unity. This condition is necessary for a good performance of the phase-lock circuitry that stabilizes the oscillator frequency on the resonance value ω_r.

3.3. The Viscometer: Mechanical Details

The device is shown schematically in Fig. 2, and consists of a flat, circular chamber with electrodes attached via a torsional rod of 0.25 cm diameter and 1.0 cm length to a base. The whole unit is made of two pieces of beryllium–copper alloy 25H, where the bottom part of the chamber is screwed into the main body. Furthermore, a thin brass ring is soldered to the joint between the two parts to enhance rigidity. The height of the fluid layer inside the cell is 0.43 mm and the diameter is 5.3 cm. Before the unit was assembled, it was hardened by heating for 3 h at 600°F. Using a lathe, the inner surfaces were polished with a succession of emery paper and optical grits down to a final grit size of 1 μm. While this did not remove all the surface characteristics, the anomalies left were concentric and we assumed that they would not cause any turbulence or lock significant amounts of fluid to the wall. This grit size of 1 μm was much smaller than the penetration depth for the fluid, $\delta \approx 9\ \mu$m. In turn, δ was much smaller than the height h. A hole of ~0.3 mm diameter through the torsion rod provided access of the fluid into the cell.

The height of the chamber was chosen as a compromise between reducing the effects of gravity, which dictate a small height, and the desire to have the fraction of the fluid in the cell much larger than in the capillaries (as will be seen later from the calculated density profile, even reducing the height by a factor of four to 0.1 mm would not have substantially reduced the effects of gravity, but the mechanical construction would have been made more difficult).

The design of the torsion rod dimensions and the chamber diameter was based on the intention to operate the oscillator at a frequency near 150 Hz, so as to have a large viscous damping from the fluid, which is proportional to $\delta^{1/2}$. The operating frequency was low enough to obtain a δ of acceptable magnitude, but large in comparison with the torsional resonance of the cradle. The choice of a lower frequency would have

a)

Capillary

Base

Torsion Bar

Electrodes

Fluid Layer

Electrode
Yoke

b)

Drive and
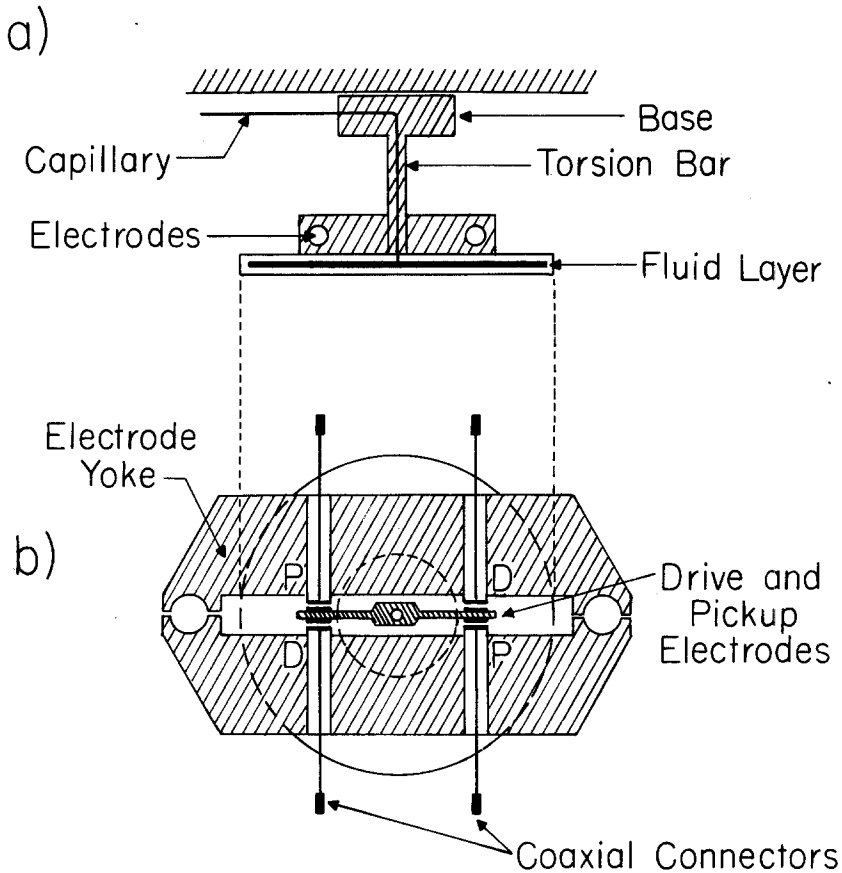Pickup
Electrodes

Coaxial Connectors

Fig. 2. Schematic presentation of the viscometer. (a) Side view showing the cylindrical base, the flat chamber, and two electrodes, biased to +200 V dc. (b) View from top with the base (dashed circle), showing the four pairs of electrodes and their support yoke.

required either a decrease of the torsion rod diameter, making the unit too fragile, or an increase in the moment of inertia, leading to less sensitivity from the fluid damping. A further design consideration was to minimize the chamber wall thickness (to decrease I_s) in such a way that a pressure of ~5 atm at 4 K inside the chamber could be supported without serious deformation.

On the two flat ears around the torsion bar above the chamber, four electrically insulated high-voltage electrodes, where a dc voltage V_{dc} was applied, were attached via Stycast epoxy. A second set of adjustable electrodes, in a copper yoke attached to the cradle, formed capacitors with each

of the four high-voltage electrodes on the viscometer shown on the diagram. A sinusoidal driving voltage V_D was applied to two diagonally opposite outer electrodes, producing only a torsional force. The induced detected voltage V_{det} was measured on the two remaining electrodes and was then fed into the regulating electronics system. In this way, the viscometer could be made to oscillate in a highly controlled way, as will be described below. The driving torque D is given by the relation

$$D = R' C_{\text{Drive}}^2 V_D V_{\text{dc}} / \varepsilon_0 A \tag{27}$$

where R' is the radial distance of the electrodes from the torsion axis, C_{drive} is the capacitance of the electrode gap, ε_0 is the permeability of space, and A is the effective surface of the electrode. The voltage induced between the detector electrodes is

$$V_{\text{det}} = \frac{2 V_{\text{dc}} R' C_{\text{det}}^2 Z}{\varepsilon_0 A^*} \omega \theta_0 \sin \omega t \tag{28}$$

where C_{det} is the capacitance of the detector electrode, Z is the impedance of a resistor between the electrodes, ω is the angular frequency, θ_0 is the oscillation amplitude, and A^* is the effective surface of the detector electrodes. The Q_T factor from which the viscosity is obtained is then found to be

$$Q_T^{-1} = \frac{D}{\theta_0 K} = G \frac{V_D}{V_{\text{det}}} V_{\text{dc}}^2 \tag{29}$$

where G is a geometrical proportionality factor that can best be determined via calibration. It was through the measurement of these three voltages that all of the viscosity data were calculated, as will be outlined in Section 4.

3.4. Viscometer Control System

To achieve frequency lock, our setup used a phase-locked loop configuration which capitalizes on the frequency-dependent phase relationship between the driving and the detected voltages in a high-Q oscillator. By means of a phase detector and an integrator, any phase lag change between the motion of the oscillator and the driving force, indicating a straying from the resonance conditions, could be converted into a voltage and fed into a voltage-controlled oscillator (VCO). The driving frequency of the viscometer would then be brought back to resonance conditions. The schematic circuit is shown in Fig. 3, where all the units except for the VCO, the integrator, and voltage regulator are of conventional design or commercially available. The simplest method of measuring V_D and V_{det} is to use the digital voltmeters
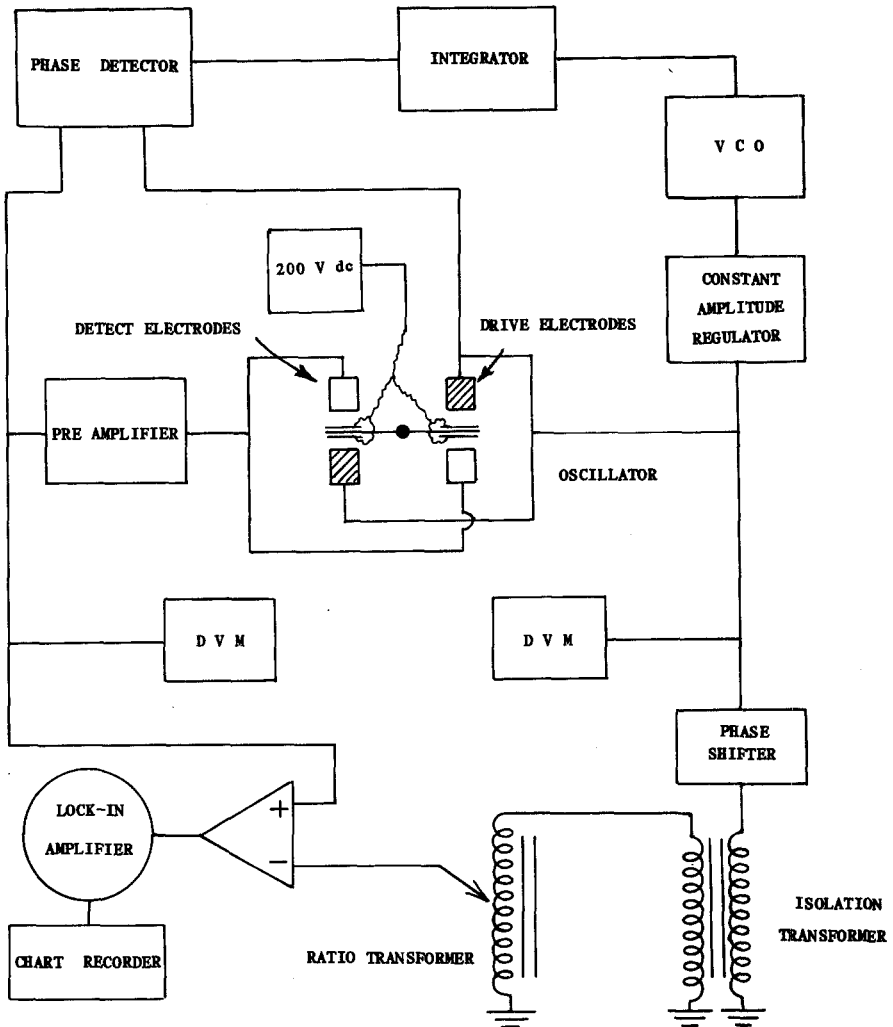
Fig. 3. Block diagram of electronic circuitry.

(DVM). In the more elaborate system indicated in Fig. 3, V_D is phase-shifted until it is in phase with V_{det}. A fraction of this voltage is bridged off by a ratio transformer and subtracted from the detected signal. A null in this subtraction, sensitively measured by the lock-in amplifier, gives a reading of the ratio V_D/V_{det} on the ratio transformer. In both arrangements, the signal-to-noise ratio made it possible to measure the ratios to within one part in 10^5.

The basic form of the VCO is that of a tuned LC circuit placed in the positive feedback loop of a high-impedance operational amplifier to make it resonate. To provide a precision voltage-controlled frequency, a variable capacitor (varactor) was placed in parallel with the main capacitor of the tuned circuit to provide the one part in 10^7 variation in frequency necessary for the fine-tuning of the high-Q viscometer. The inductor in the LC circuit was simulated by operational amplifiers placed in the form of a gyrator circuit.[34] In this way a nearly ideal LC oscillator with a clean, stable sine wave was produced to drive the viscometer. Details of the design are given in Ref. 35.

3.5. Cryostat Temperature Measurement and Control

Two germanium resistors (Cryocal 2500H) were placed in the cradle as indicated in Fig. 1. They were calibrated between 4.2 and 1.7 K by means of a ^{4}He vapor pressure thermometer attached to the cradle as indicated in Fig. 1. The T-58 ^{4}He temperature scale was then used as our primary standard. An additional Cryocal GE resistor, commercially calibrated for the range between 4 and 20 K, was used to calibrate the two other GE resistors above 4 K. A bridge circuit comprising an audio generator with fine voltage control, ratio transformer bridge, and phase sensitive detector, together with a servoheater, permitted the control of the temperature to $\sim 1\ \mu$K. During these measurements, the ac excitation voltage across the bridge, ~ 28 mV rms, was kept constant within 0.1% to avoid drifts caused by the very sensitive dependence of the thermometer resistance on the heating current.

The density cell was of a standard design, including two insulated horizontal plates rigidly mounted in a copper casing, where all the fluid was contained within a height of ~ 0.3 mm. The dielectric constant of the fluid was measured by means of a ratio transformer bridge system, and the Clausius–Mossotti relation with a polarizability $\alpha = 0.1233$ cm^3/mole was used[36] to calculate the density. A standard capacitor for the second arm of the bridge was thermally anchored on the cradle near the density cell. Density resolutions $\delta\rho/\rho \sim 10^{-6}$ were routinely achieved. Corrections were made to the measurement for the bowing of the capacitor plates from the effects of the pressure. This correction was determined by measuring the dielectric constant of ^{4}He at 77 K at a number of pressures between 0 and 3 atm, and by assuming that at this temperature, ^{4}He behaves like an ideal gas. This measurement gave the change of the capacitor geometry with pressure at 77 K and was assumed to be also valid at 4 K. The correction to the density from this source accounted for ~ 0.5% of the total measurement, and we estimate the absolute value of the density to be correct to within the published uncertainty in the polarizability, ~ 0.1%.

4. EXPERIMENTAL PROCEDURE

Two purposes are served in this section. First, an outline is given of the relevant steps used to prepare the system and to control the operation of the viscometer. Second, a number of calculations are performed to show that the measurements are performed under linear conditions.

4.1. Viscometer Operation

Beginning at room temperature and atmospheric pressure, a Q_E for the empty cell of approximately 10^3 could be achieved by judicious placement of the various leads in the vicinity of the viscometer, rigid mounting of all accessories on the cradle, and careful preparation of the electrodes. This optimization could be reached only by tedious trial and error. Following this, Q_E reached $\sim 6 \times 10^4$ in vacuum. As the cradle was cooled to 77 K, Q_E increased by a factor of approximately 3, and again by ~ 3 after further cooling to 4 K. This resulted in a final value of $Q_E \sim 5 \times 10^5$, where some variations between series of experiments were seen after modifications of the electrodes had been made. In the region between 10 and 1.7 K, experiments were conducted where the ratio V_D/V_{det} was measured and the free decay curve was obtained to establish that there was no appreciable temperature dependence of Q_E. Once this check had been made, helium was introduced into the cell and a $Q_T \sim 3 \times 10^4$ was reached. No departure from a truly exponential decay could then be observed from an analysis of V_{det} versus time. This last exercise was repeated from time to time at a number of temperatures and in particular close to the critical point, but the decay was always found to be exponential.

Another test was to see whether the filled viscometer was oscillating in a linear response regime or whether it was overdriven. Besides the test of the exponential decay with time, we studied the ratio V_D/V_{det} as a function of V_D by varying V_D by a factor of up to 20. We found that this ratio did not change more than 0.2%, proving again that we were operating under linear oscillation conditions.

4.2. Sample Preparation and Viscosity Measurements

In order to locate the critical isochore, density data along an isotherm $\varepsilon \approx 10^{-2}$ were taken as a function of pressure. From previous experiments on ^{3}He,[9] and also from the scaling theory,[20] the chemical potential derivative $(\partial \mu / \partial \rho)_T^{-1} = \rho^2 \beta_T$, where β_T is the compressibility, is a symmetric function of $|\rho - \rho_c|$ with a maximum at ρ_c. This was again verified for a number of isotherms both for ^{3}He and ^{4}He. The critical density, located within 0.3%, was found to be 0.0414 and 0.0700 g/cm,^{3} in very good agreement with previous measurements.[9,37]

A series of viscosity measurements along isochores was then started by filling the viscometer at $\varepsilon \simeq 10^{-2}$ to a density $\rho/\rho_c \simeq 1.20$ as indicated by a reading of the density cell. Ample time was allowed to permit an equilibrium between the two cells. The valve of the viscometer was then closed and the ratio V_D/V_{det} was measured, using regularly spaced reduced temperature intervals. The output of the ratio transformer detection bridge was displayed on a chart recorder as a function of time and served as an indication of the equilibration process. In this way, measurements along several isochores were taken by successively decreasing the density in the viscosity cell by steps of 1-3%, depending on the proximity to ρ_c.

The indication that the coexistence curve was reached, after starting from the single-phase region, was an anomalous change in the ratio V_D/V_{det} with temperature. Away from the critical isochore, this change was sharp, but for near-critical isochores, $|\rho - \rho_c|/\rho_c \lesssim 0.02$, the ratio V_D/V_P passed through a fairly broad maximum as a function of temperature, thus preventing a precise location of the critical point. The broad maximum is a result of the earth's gravitational field and will be discussed in detail in Section 5. We have attempted to locate T_c more precisely by observing whether the equilibration time after small, regularly spaced temperature steps near T_c showed a sharp change with T. Unlike the situation of calorimetric measurements,[10,38] where the thermal relaxation time changed drastically when T_c was reached and permitted an accurate location of T_c, no such evidence was found. Hence, the final determination of T_c had to be done by means of a model, as will be described in Section 5.

At the high-temperature end, far above T_c, we were limited by the maximum pressure the viscometer could withstand. We arbitrarily set a limit of 5 atm as our maximum pressure, which corresponded to a maximum temperature of 5.5 and 7.0 K for ^{3}He and ^{4}He, respectively.

Viscosity measurements along isotherms were impractical, because of the long equilibration times encountered in transferring fluid between the room-temperature containers and the viscometer. These times became particularly long near the critical isochore and near T_c, of the order of several hours. However, the shifts between the viscosity measurements along isochores on a given series of measurements were small enough that, by data interpolation, values of η along isotherms could be calculated and they showed only small scatter, as will be discussed in Section 5.

4.3. The Shear Rate

We have calculated the maximum shear rate $S = \partial v_r/\partial z$ for the fluid, where v_r is the velocity of the oscillating disk at the distance r from the axis. We have approximated the shear rate to $S = \bar{v}_r/\lambda$, where $\bar{v}_r = \omega\theta_0 R$ is

the rms velocity. To calculate θ_0, we have measured the capacitance near the electrodes and its change under the application of an ac voltage. We have found that under the conditions where oscillations were stable, the amplitude is $3 \times 10^{-6} < \theta_0 < 5 \times 10^{-4}$ rad for $2 < V_{det} < 200$ mV and $V_{dc} = 200$ V. Using values for ^{3}He of $\eta = 16 \mu$P, $\rho = 0.04$ g/cm^3, $\omega/2\pi = 1.6 \times 10^2$ Hz, and $R = 2.5$ cm, we calculate $5 \times 10^{-1} < S < 50$ sec^{-1} over the linear range of the oscillation, where the lower value indicates the limit of stable oscillator operation. Usually, we have performed the experiments with $\theta_0 \simeq 1 \times 10^{-4}$ rad.

We have compared this shear rate with the average decay rate $\bar{\Gamma}$ of the fluctuations near the critical point, given by Eq. (11). To avoid deformation of the fluctuations in the fluid, the shear displacement l over a length ξ in a time $\bar{\tau}^{-1}$ in the fluid, given by $l = \bar{\Gamma}^{-1} \delta v_r = \xi S \Gamma^{-1}$, should always be smaller than ξ; hence, we require $S < \bar{\Gamma}$. Substituting numerical values for ^{3}He, namely $\eta \sim 16 \mu$P, the correlation length along the critical isochore $\bar{\rho} = \rho_c$, $\xi = 2.7 \times 10^{-8} \varepsilon^{-\nu}$ cm, with $\nu = 0.63$, and $T = 3.31$ K into Eq. (11), we find that for $\varepsilon \gtrsim 5 \times 10^{-5}$ the condition $S < \bar{\Gamma}$ is satisfied. However, as we shall see below, gravity effects dominate the observed viscosity data for $\varepsilon < 10^{-4}$, and under experimental conditions, ξ at a given ε is much smaller along the walls of the viscometer than indicated by the above equation. Hence, in practice, the condition $S < \Gamma$ is always satisfied for $\bar{\rho} = \rho_c$ over the whole temperature range used, i.e., for $\varepsilon > 10^{-6}$. However, for $|1 - \rho/\rho_c|/\rho_c \simeq 0.02$, the density at one of the horizontal walls of the cell can become quite close to ρ_c due to gravity, as will be shown later. Then ξ can reach values close to those along the critical isochore, and under these circumstances the condition $S < \bar{\Gamma}$ might no longer be satisfied for $\varepsilon \lesssim 10^{-5}$.

4.4. Power Dissipation

The total power dissipated in the viscometer is given by the relation[39]

$$\dot{E} = \frac{1}{2} \eta \frac{\rho\omega}{2} \int u_0^2 \, ds \tag{30}$$

where u_0 is the linear velocity amplitude at the fluid boundary, while the integral is over the surface of contact, giving for the two parallel circular plates with the vertical wall of height h

$$\dot{E} = \frac{1}{4} \pi\rho\eta\omega^2 \theta_0^2 R^3 (R + 2h) \tag{31}$$

Using the same operational parameters for ^{3}He as in Section 4.3, we obtain $\dot{E} = 6 \times 10^{-2}$ erg/sec. Taking for the thermal conductivity of Be–Cu at 4.2 K

the value[40] of $\lambda = 0.019$ W/cm K, we find that this power dissipation leads to a temperature difference of $\Delta T \sim 2\,\mu$ K between the viscometer body and the cradle.

4.5. Viscometer Calibration

Two methods were used to calculate the absolute viscosity from our V_D/V_{det} data. The first consisted in measuring the free decay of the oscillations after switching off the driving ac voltage and determinging τ from the least squares fit to an exponential. Using Eq. (25), we obtained Q_T. Furthermore, knowing the empty-cell Q_E and the moment of inertia I_s, calculated from the viscometer geometry, we could calculate the viscosity from Eq. (26). In turn, the resulting value for Q_T, combined with the recorded value of V_D/V_{det} before the free decay, permitted determination of the geometrical parameter G in Eq. (29). Although this is the most direct method of calibration, the calculation involves determining accurately the surface area inside the chamber and the moment of inertia of the solid parts, which was considered to be uncertain to about 3% because of the difficulty in estimating accurately the moment of inertia due to the solder on the outer ring.

An alternate method consisted in calibrating the viscometer using ^{4}He under saturated vapor pressure at the superfluid transition, where the absolute viscosity has been reported by several authors.[41] Of course, this calibration is only as accurate as these prior measurements. The drawback of this method was the uncertainty about the absolute value of $\eta(T_\lambda)$ for the two most recent and apparently most precise viscosity measurements by Biskeborn and Guernsey[31] and Bruschi et al.[42] In Ref. 31, where a torsional oscillator was used, the reported value was $\eta(T_\lambda) = 27 \pm 1\,\mu$P, which is significantly higher than those of previous measurements quoted by Ahlers,[41] where on the average $\eta(T_\lambda) = 24.7\,\mu$P. The measurements of Ref. 42, done with a vibrating wire, did not yield the absolute value of η, but rather the ratio $\eta\rho_n/(\eta\rho)_{T_\lambda}$, where ρ_n is the density of the normal fluid. We note that just as with the torsional oscillator, the experiment with a vibrating wire measures the product $\eta\rho_n$.

To first check how our data compare with those of Refs. 31 and 42, we plotted in Fig. 4 the normalized product $\eta\rho_n/(\eta\rho)_{T_\lambda}$ versus T. Our system was not designed for measurements under saturated vapor pressure, and our pressure was kept constant at 7 cm Hg. The scatter of our data was found comparable with that of Bruschi et al., and the agreement on the whole is satisfactory. This reinforces our conjecture that our viscosity measurements are reliable on a normalized scale. We leave to a future publication a more sensitive comparison with the data of Refs. 31 and 42, which is beyond the scope of the present paper.
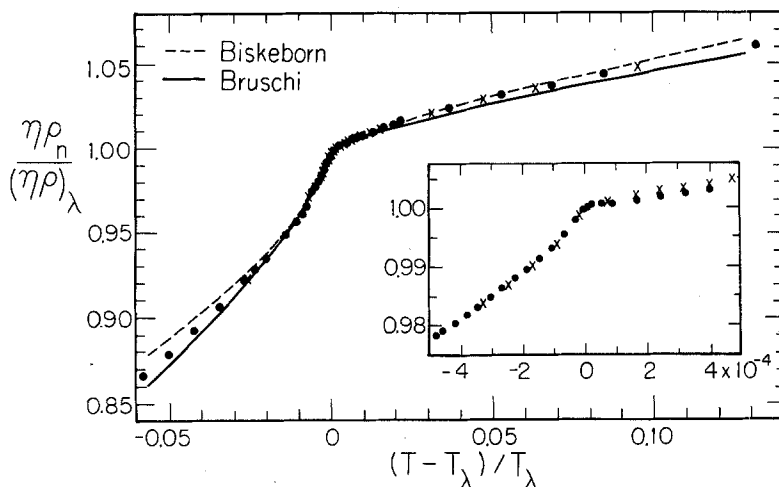
Fig. 4. The normalized viscosity $\eta\rho_n/(\eta\rho)_{T_\lambda}$ near the superfluid transition of ^{4}He. ($\bullet$, $\times$) Present data taken on two series of experiments. (—) Bruschi et al.[42] (--) Biskeborn and Guernsey.[31] The insert shows the region close to T_λ in more detail.

We calculated the absolute viscosity of ^{4}He at T_λ using our first method and obtained $\eta = 26.0 \pm 1.0 \, \mu$P, where we used $\rho(T_\lambda) = 0.1462 \, \text{g/cm}^3$ as determined with our density cell.

We finally adopted as a compromise the value of $\eta(T_\lambda) = 25.1 \, \mu$P from the published value by Webeler and Allen,[43] who were quoted by Ahlers.[41] This determination permitted the calculation of the geometrical factor G of the viscometer and hence the absolute value of η for any helium mixture in the temperature range below 10 K, where this factor was constant.

In summary, the stability achieved with the viscometer system permits measurements with a scatter in η that is determined by the reproducibility and the stability of the ratio V_D/V_{det}. This scatter is of the order of 0.05%, which is comparable with that for the best available viscosity measurements.[31,42,43] The absolute viscosity is determined only to $\pm 3\%$ because of uncertainty in the oscillator geometry, but possibly better from calibration at the lambda point of ^{4}He using previous data.

5. MODEL CALCULATIONS OF THE APPARENT VISCOSITY

Gravity profoundly influences the measurement of properties near a liquid–vapor critical point[21] and prevents observing their intrinsic asymptotic behavior. The situation in viscosity measurements using a layer of a finite height is special because the torsional oscillator system only

measures effectively the product $\rho\eta$ for the layers of depth λ in the top and bottom plates (we neglect the small contribution from the vertical wall). This contrasts with the other experiments, such as thermal conductivity, specific heat, density, etc., where measurement from an integration over the whole sample thickness is made.

Hence it is advantageous, before presenting the data, to predict how the measurements are most likely going to be affected by gravity. The most useful results are (1) the intrinsic viscosity distribution inside the fluid layer for a given average density $\bar{\rho}$ and ε, and (2) the prediction of the temperature shift of the experimental viscosity maximum (or discontinuity) with respect to that of the coexistence curve. It is also useful to determine numerically the temperature dependence of the critical viscosity under conditions of smaller gravity than on earth, and then to calculate the predicted frequency dependence of η in the critical regime.

For these calculations, it is most appropriate to present the ratio $\eta/\bar{\eta}$ instead of the absolute viscosity, and for these model calculations we are using values for parameters from properties determined experimentally, as presented in Table I, together with the restricted cubic model for the equation of state.[20] The derivative $(\partial P/\partial T)_\rho$, needed for this calculation [see Eq. (4)] both as a function of ρ and ε, was obtained from the data of Refs. 9, 37, and 44 for ^{3}He, ^{4}He, and CO_2. The amplitude ξ_0 of the correlation length was taken from the two-scale factor universality,[45] which for ^{3}He

TABLE I

Parameters Used for the Calculation of the Viscosity $\tilde{\eta}/\bar{\eta}$ and of the Singular Conductivity $\Delta\lambda$ Using the MC Expressions by Olchowy and Sengers[13a]

	^{3}He	^{4}He	CO_2
a	4.05	5.66	18.9
k	0.818	0.904	1.273
ξ_0 Å	2.6	2.0	1.6
$\lambda(\rho_c)$, ergs/sec cm. K	$940 + 163\,T^b$	$1020 + 136\,T^c$	5.45×10^{3d}
$\bar{\eta}(\rho_c)$, μP	16.7^e	$19.1 + 0.83\,T^e$	341^f
P_c dynes/cm^2	1.146×10^6	2.274×10^6	7.375×10^7
ρ_c gr/cm^3	0.04145	0.0696	0.4678
T_c K	3.309	5.1895	394.13

$\alpha = 0.100$, $\beta = 0.355$, $\gamma = 1.190$, $\nu = 0.633$, $\delta = 4.352$, $b^2 = 1.310$, $c = 0.0393$

[a] The coefficients a and k are fluid-dependent parameters from the cubic model, $b^2 = 3(3-2\beta)^{-1}$, $c = (2\beta\delta - 3)(3-2\beta)^{-1}$, given in Table 4.3.4 of Ref. 20. The exponents, as well as ξ_0, P_c, ρ_c, and T_c, are also those presented in Ref. 20.
[b] Ref. 12.
[c] Ref. 49.
[d] Ref. 50.
[e] This work.
[f] Ref. 7.

and ^{4}He is in good agreement with data from acoustic attenuation measurements, $(2.6 \pm 0.3) \times 10^{-8}$ and $(1.8 \pm 0.4) \times 10^{-8}$ cm.[46] The specific heat C_v data for ^{3}He, ^{4}He, and CO_2 along the critical isochore were taken from Refs. 10, 47, and 48. The background heat conductivity $\bar{\lambda}(\rho_c, T)$ for ^{3}He and ^{4}He was from an analysis of data from Refs. 12 and 49, and for CO_2 was obtained from the data by Michels et al.[50] The background viscosity data $\bar{\eta}(\rho_c, T)$ for ^{3}He and ^{4}He are from the present work, and those for CO_2 are from Bruschi and Torzo.[7] It is to be noted that the critical exponents are not the asymptotic ones, but rather the effective ones determined over the temperature range above $\varepsilon \sim 10^{-4}$, where the bulk of the measurements were taken. In this section, we shall only discuss calculations for ^{3}He, but the parameters for ^{4}He and CO_2 will be used in the data analysis of Section 6, where we discuss the viscosity measurements.[7]

Generally, as for the other diverging properties in a fluid near the critical point, we can foresee several regimes.

(a) Above T_c, say for $\varepsilon > 10^{-1}$, the viscosity will have a "background" behavior, $\bar{\eta} = f(\rho, T)$, where the variations with temperature will be monotonic.

(b) Closer to T_c, roughly for $10^{-3} < \varepsilon \le 10^{-1}$, lies the crossover regime from the background into the asymptotic "power law" behavior.

(c) Still closer to T_c, for $\varepsilon < 10^{-3}$, the power law behavior should emerge. It is in this regime that the measurements become progressively affected by gravity as T_c is approached. The temperature when this influence becomes important is determined by the height of the fluid layer and by the static properties of the fluid.[21]

5.1. The Gravity Effect

We first note that, according to Eq. (26), the viscometer system measures a quality factor Q_F such that $Q_F^{-1} \propto \sum (\eta \rho)^{1/2}$, where the summation is over the contribution from top and bottom plates. Let us consider a fluid with an average density $\bar{\rho}$ and a background viscosity $\bar{\eta}$ far above T_c, where the gravity effects are negligible. Then we define a "background" $\bar{Q}_F$

$$\bar{Q}_F^{-1} \propto 2(\bar{\eta}\bar{\rho})^{1/2} \qquad (32)$$

where the factor 2 accounts for the top and bottom plates. Closer to T_c there will be a vertical density gradient, leading in turn to a viscosity gradient, and we will have for our equal top and bottom plate geometry

$$Q_F^{-1} \propto [(\rho_t \eta_t)^{1/2} + (\rho_b \eta_b)^{1/2}] \qquad (33)$$

where the subscripts t and b denote top and bottom. Hence, forming the

measured ratio, we have

$$\frac{\bar{Q}_F}{Q_F} = \frac{(\eta_t \rho_t / 2\bar{\rho})^{1/2} + (\eta_b \rho_b / 2\bar{\rho})^{1/2}}{\bar{\eta}^{1/2}} \equiv \left(\frac{\tilde{\eta}}{\bar{\eta}}\right)^{1/2} \tag{34}$$

where $\tilde{\eta}$ is a weighted average viscosity that is the measured quantity. In the absence of gravity, the above expression would give the ratio of the intrinsic viscosities $\eta / \bar{\eta}$.

Hence, the procedure followed in this part to calculate $\tilde{\eta}$ consists in first determining the vertical density profile in the fluid for the density $\bar{\rho}/\rho_c$ as a function of the reduced temperature. For this program, we have followed the approach by Hohenberg and Barmatz,[51] using the cubic model set of equations with the polar coordinates r and θ.[20] An outline of these equations and the method of determining ρ/ρ_c for a given $\bar{\rho}$ is presented in Appendix D. The solution by numerical methods of these equations gives all the static properties via the parameters r and θ, and in particular we have the relation[21]

$$\xi = \xi_0 r^{-\nu}(1 + 0.16 \, \theta^2) \tag{35}$$

so in effect we have obtained ξ as a function of ρ and ε. Second, η and furthermore the composite value $\tilde{\eta}/\bar{\eta}$ are calculated as a function of ρ and ξ using the MC expressions developed by Olchowy and Sengers together with the parameters in Table I.

Here three remarks are in order: (a) the cubic model is essentially geared to the asymptotic regime for the static properties, where the critical exponents α, β, γ, etc., are constant and obey the scaling relations. However, the application to the viscosity problem involves a temperature range $10^{-5} \lesssim \varepsilon \lesssim 10^{-2}$ for the gravity effect, where the critical exponents have taken an effective value somewhat different from the asymptotic one. The values listed in Table I represent the best available ones of the effective exponents over this range, made internally consistent with the scaling relations. (b) the parameter $q_D = 3 \times 10^6 \, \text{cm}^{-1}$ for ^3He, not listed in Table I, was used for this model because, as we shall see later in the result analysis, it represents the viscosity data very well. (c) We emphasize that the ratio $\tilde{\eta}/\bar{\eta}$, to be presented in several figures throughout this paper, represents a weighted average that reduces to the intrinsic value of $\eta/\bar{\eta}$ when gravity effects have become negligible, namely for $\varepsilon \gtrsim 2 \times 10^{-4}$.

To help in visualizing the effect of gravity, we plot in Figs. 5 and 6 a vertical profile of the density and of the intrinsic viscosity η for the experimental cell of 0.43 cm height, and we also show by two solid marks near the bottom the size of the penetration depth δ. As representative average densities, we have used $\bar{\Delta}\rho \equiv (\bar{\rho} - \rho_c)/\rho_c = 0$ and -0.03. In both figures one notes that for $\varepsilon \gtrsim 10^{-3}$, where the density gradients have not yet developed, the viscosity is almost constant throughout the cell. However, at smaller
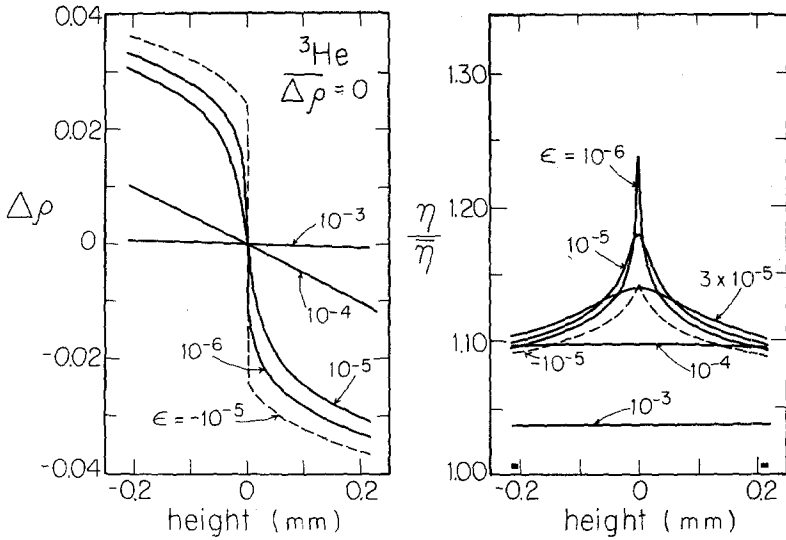
Fig. 5. (a) The vertical density profile at several values of ε for $\overline{\Delta\rho} = 0$ in the cell of height $h = 0.43$ mm. (b) The corresponding vertical viscosity profile at the same values of ε as in (a). The solid horizontal bars near the "height" axis indicate the penetration depth δ at the top and bottom of the cell.

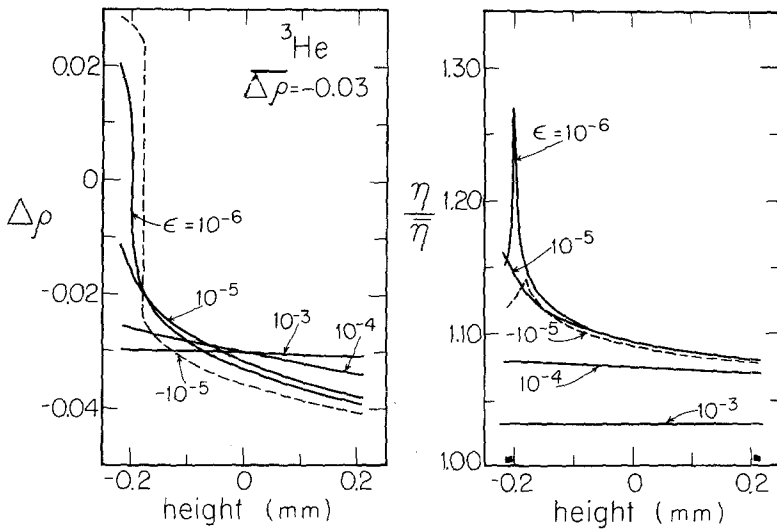Fig. 6. (a) The vertical density profile at several values of ε for $\overline{\Delta\rho} = -0.03$. (b) The corresponding vertical viscosity profile at the same values of ε as in (a). The solid horizontal bars near the height axis indicate the penetration depth δ at the top and bottom of the cell.

reduced temperatures, where some specific layer has a density close to ρ_c, a sharp viscosity peak develops around this layer, although it cannot necessarily be measured. As ε changes, so does the vertical position of the layer $\rho = \rho_c$ when the average $\bar{\rho}$ is different from ρ_c.

In these viscosity measurements, an effect similar to that encountered with the specific heat c_v is produced, and this is shown in Fig. 7, where we plot the ratio $\tilde{\eta}/\bar{\eta}$ versus ε on the critical isochore. The peak of $\tilde{\eta}$ does not coincide with T_c, but is situated at $\varepsilon \approx 4 \times 10^{-5}$, nearly 150 μK above T_c. (In specific heat experiments, by contrast, the C_V peak is predicted[51] and observed[10,52] below T_c.) As can be seen, gravity effects under earth conditions become visible for $\varepsilon \lesssim 2 \times 10^{-4}$. For comparison, we also present the calculation when the earth's gravity field g_0 has been reduced by a factor of 10^3.

This calculation was done using a critical exponent $z_\eta = 0.054$. Hence, on a logarithmic plot of $\tilde{\eta}/\bar{\eta}$ versus ε, the asymptotic slope, according to Eq. (6), would be expected to be $z_\eta \nu = 0.0342$. In reality, the weak -
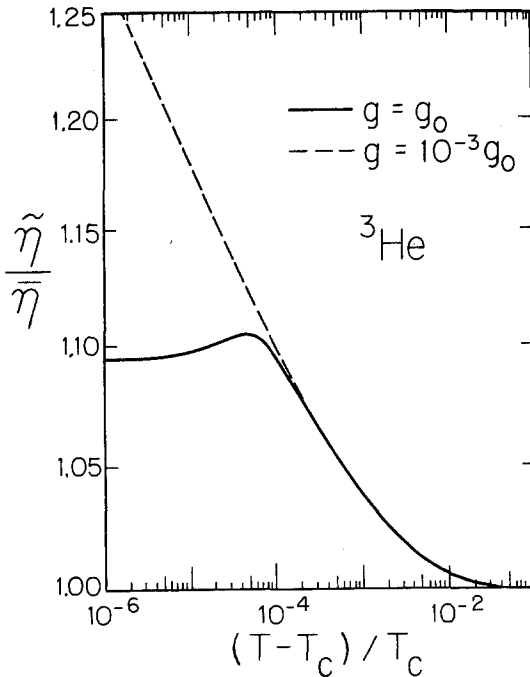
Fig. 7. The normalized effective viscosity $\tilde{\eta}/\bar{\eta}$, to be measured in the cell, versus ε along the critical isochore $\rho = \rho_c$. (—) With $g = g_0 = 9.80 \times 10^2$ cm/sec^2 (earth's gravity). (- -) With $g = g_0 \times 10^{-3}$.

temperature dependence of the factor Q produces a relation of the form of Eq. (7) with $z_\eta(\text{eff})\nu = 0.0327$, as a numerical analysis of the model calculation shows.

Another interesting feature of the model calculation under normal gravity conditions is the large temperature range of the crossover regime. Along with the gravity-dominated region, this leaves hardly any section where we can see a purely power law behavior for the viscosity, namely a straight line on this logarithmic plot. We also note that the singular behavior
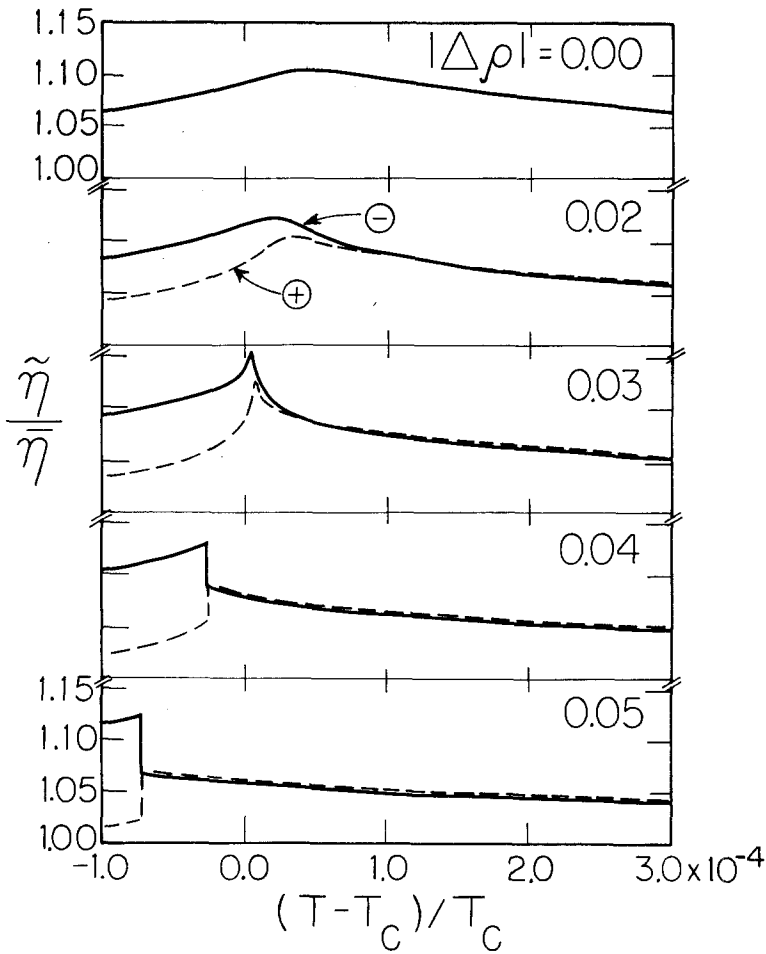
Fig. 8. The effective calculated normalized viscosity $\tilde{\eta}/\bar{\eta}$ to be measured in the cell versus ε close to the coexistence curve and along several isochores. (—) $\Delta\rho < 0$, (--) $\Delta\rho > 0$.

is a weak effect starting at less than $\varepsilon = 10^{-1}$ and not rising beyond 10% over the background for the maximum value.

We now examine in Fig. 8 the viscosity model calculation for $\tilde{\eta}/\bar{\eta}$ along several near-critical isochores in ^{3}He, where we have used a linear scale for the reduced temperature, focusing on the region where the transition from the single-phase into the coexistence region is to occur. The dashed and the solid lines express isochores with $\bar{\Delta}\rho > 0$ and $\bar{\Delta}\rho < 0$. What is particularly striking is that the highest peaks do not occur on the critical isochore, but rather when the average density is $|\Delta\rho| \simeq 0.03$. This phenomenon is to be expected from our discussion centering on Figs. 5 and 6. At a temperature close to T_c, density gradients become important. Then, for $\bar{\Delta}\rho = 0.03$ the density very close to the top horizontal wall is close to ρ_c, and for $\bar{\Delta}\rho = -0.03$, $\rho \approx \rho_c$ near the bottom wall. At these places, the viscosity is then highest.

Further away from the critical density, a different phenomenon takes place, which produces the sharp changes in the curves in Fig. 8. Here the meniscus forms at one of the walls by the appearance of a liquid layer ($\bar{\rho} < \rho_c$) or a vapor layer ($\bar{\rho} > \rho_c$). For the droplet, the product $\rho\eta$ is larger than for the fluid at the opposite wall and $\tilde{\eta}/\bar{\eta}$ will rise sharply as T decreases. For the bubble, the opposite phenomenon is produced.

Finally, we show in Fig. 9 the expected frequency effect on the viscosity in the absence of gravity, calculated from Eq. (10) along the critical isochore.
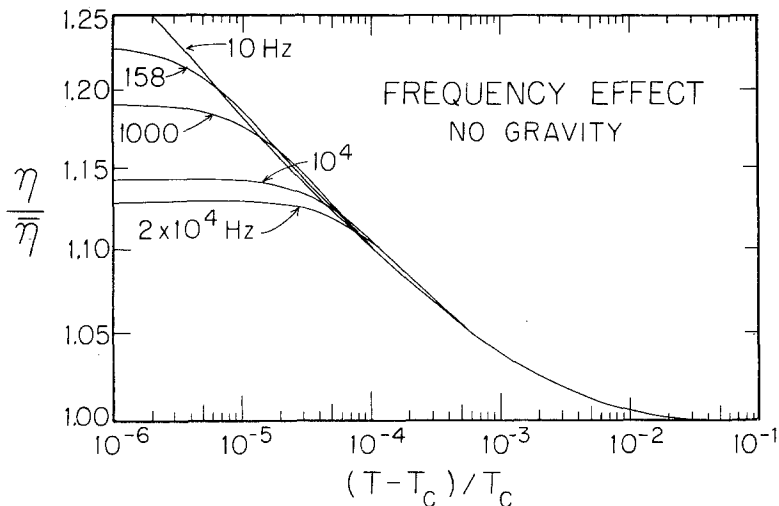

Fig. 9. Calculated normalized viscosity under zero gravity versus ε at several frequencies.

For our resonant frequency, the viscosity divergence begins to roll over at a reduced temperature of $\varepsilon \simeq 10^{-5}$, when Γ becomes comparable to ω. Comparing this figure with Fig. 7, where the effects of gravity are seen, it is clear that frequency effects will be obscured by gravity effects. It is only at higher frequencies than 10^4 Hz, which are unsuitable for a torsional oscillator, that frequency effects can be studied. In the low-gravity environment offered by the space shuttle, not only will the intrinsic viscosity be measured, but comparison between torsional oscillators at 10^2 and 10^4 Hz should be able to demonstrate very clearly the predicted frequency effect.

6. EXPERIMENTAL RESULTS

Our data for ^{3}He and ^{4}He were obtained along a number of isochores in several series of experiments. In each series, a calibration with ^{4}He at T_λ was carried out. The data points, tabulated as absolute and normalized viscosity $\tilde{\eta}$ and $\tilde{\eta}/\bar{\eta}$ versus ε, are available from one of the authors (H.M.).

In this section, we first present a general view of the data and a discussion of the background viscosity for the particular case of the critical isochore. This is followed by a presentation of the reduced viscosity $\tilde{\eta}/\bar{\eta}$ along the critical isochore and along several isotherms, along with the fit of the MC model theory, including gravity effects, to these data. In addition, we use the same approach to fit the critical conductivity to the experimental data. Finally, we make a similar analysis of the CO_2 viscosity data[7] and compare the results to those for the helium isotopes. A plot of the ^{3}He viscosity data to exhibit the asymptotic and the leading correction-to-scaling term[4] is also presented.

6.1. The Background Viscosity

In Fig. 10 a general view of the viscosity data for ^{3}He is shown on a linear reduced temperature scale. From the 29 isochores measured in three series, we present only 16 from one series to avoid overcrowding. It can be seen that the singular part of the viscosity is largest for densities near the critical one, but not at ρ_c itself. Furthermore, the background viscosity increases with density.

A more detailed view is presented in Fig. 11, where we plot $\tilde{\eta}$ along several isochores for ^{3}He, including the critical one, on a linear temperature scale. We note the density-dependent temperature variation of the background contribution $\bar{\eta}$, where, for the critical isochore, the slope $d\bar{\eta}/dT$ is nearly zero over a large temperature region. Also, we note the behavior near the coexistence curve: a sharp rise with a peak is observed as the critical point is approached. For isochores well above (respectively below) the critical one, the rise is much smaller and there is in addition a sharp
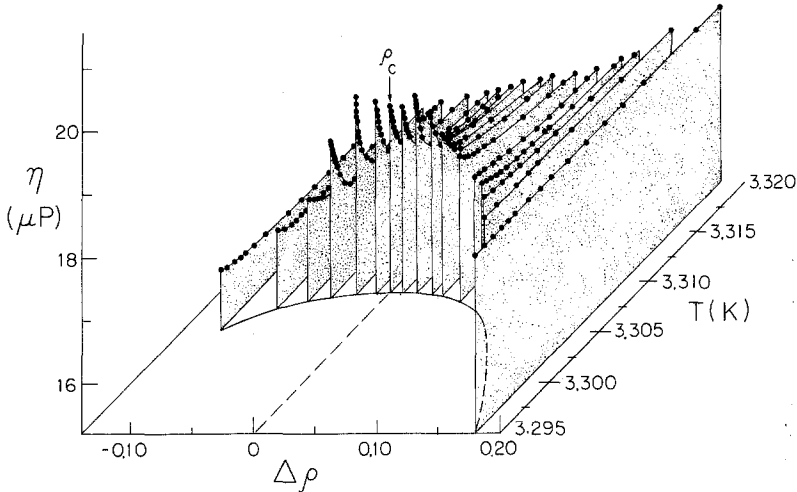
Fig. 10. General view of the absolute viscosity data for ^{3}He versus ε along selected isochores from a total of 17 isochores in a single series.

jump upward (or downward) shown by vertical lines, as the transition into the two-phase region takes place. This is just as the model in Section 5 predicted. In Fig. 11, we also show for comparison the behavior of ^{4}He along the critical isochore where the background slope $d\bar{\eta}/dT$ is much larger than for ^{3}He. This different behavior was reproducible in several series of measurements between which the cryostat was warmed up. In Fig. 12 we show the background $\bar{\eta}(\rho)$ near T_c plotted versus ρ in two series of experiments between which the cell was repaired. In the second series, no new calibration with ^{4}He at the superfluid transition was made, and yet the absolute viscosity measurements differ by only 1.3%, which is smaller than the systematic uncertainty.

For our data analysis, we have fitted the background viscosity to polynomials of the form

$$\bar{\eta}(\rho, T) = A(\rho) + B(\rho)T + C(\rho)T^2 \qquad (36)$$

A tabulation of the coefficients $A(\rho)$, $B(\rho)$, and $C(\rho)$ is available on request. The estimation of the background viscosity close to T_c is crucial in determining the shape of $\tilde{\eta}/\bar{\eta}$ versus ε, to be discussed in Section 6.2, and hence the value of the fit parameters. There is always some ambiguity on the separation of $\bar{\eta}$ from the total η, which in turn leads to a systematic uncertainty in the fit parameters—as distinct from their precision—and which is difficult to estimate.

Predictions of $\bar{\eta}$ in gaseous helium, presumably at very low pressures, have been made by De Boer[53] and De Boer and Cohen,[54] using quantum
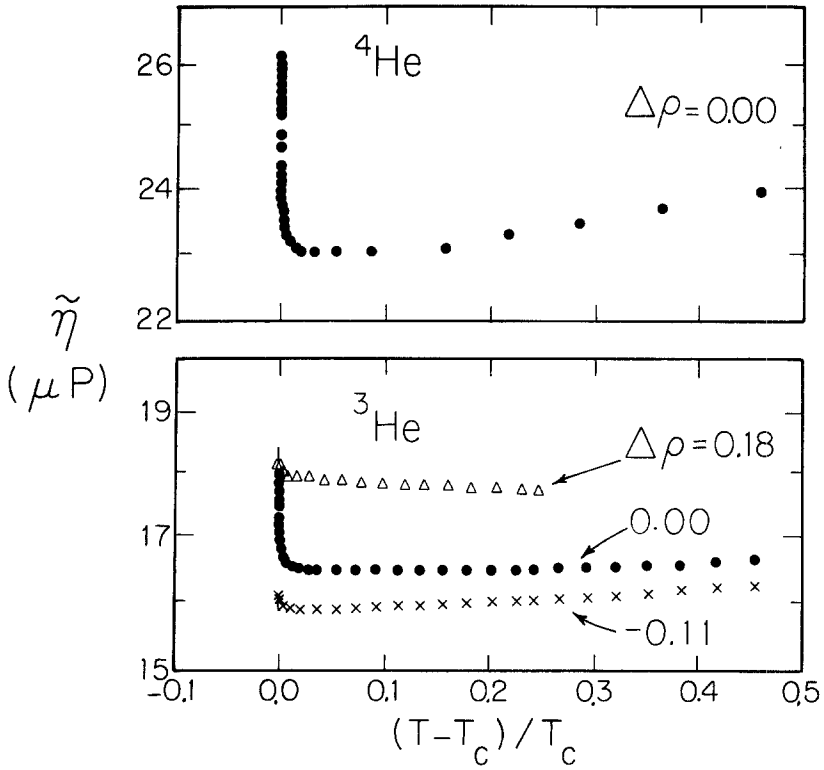
Fig. 11. The absolute viscosity of ^{3}He and ^{4}He versus ε along a few isochores. The vertical scale is logarithmic.

mechanically correct Boltzmann transport equations. Unfortunately, the calculations on ^{4}He only extend up to ~3 K. Those for ^{3}He give $\eta \simeq 12.5 \ \mu$P near zero pressure. Our data for ^{3}He using densities $0.9 < \rho/\rho_c < 1.2$ and an isochore $\rho/\rho_c = 0.50$, give $\eta \approx 11 \ \mu$P by extrapolation to $\rho = 0$. However, it is not clear how justified such an extrapolation is, and more data at intermediate densities are needed. Nevertheless, the results are not inconsistent with predictions.[54]

A more complete discussion of the background viscosity will be presented elsewhere, together with extensive data on ^{3}He–^{4}He mixtures along a number of isochores near the critical line.[55]

6.2. The Critical Viscosity Along ρ_c

From our observations in Sections 4 and 5, it is clear that viscosity experiments do not sharply locate the critical point either from the viscosity peak or from any sudden change in the observed equilibration time.
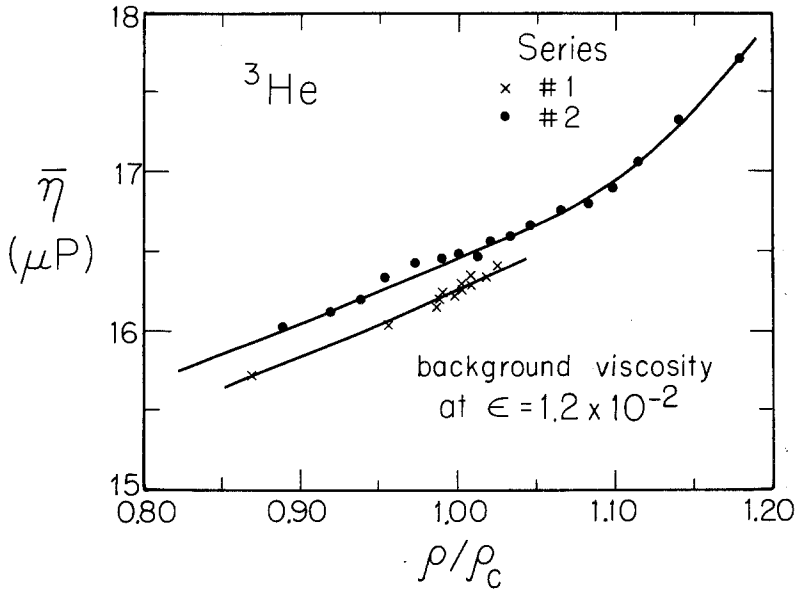
Fig. 12. The background viscosity of ^{3}He at $\varepsilon = 1.1 \times 10^{-2}$ versus the normalized density ρ/ρ_c from two series of measurements.

However, model calculations predict that the observed peak in $\tilde{\eta}$ is shifted above T_c by $\delta\varepsilon_{\text{peak}} = (4.0 \pm 0.5) \times 10^{-5}$ and $(3.0 \pm 0.5) \times 10^{-5}$ for ^{3}He and ^{4}He, respectively. The quoted uncertainty was estimated from a number of calculations using different values for the critical exponents and cubic model parameters from those of Table I, so as to reflect more closely the asymptotic conditions. Also, the exponent z_η was varied between 0.054 and 0.065. In our data presentation, we will therefore shift the observed peak by the predicted amount.

In Fig. 13 we show the normalized viscosity $\tilde{\eta}/\bar{\eta}$ versus ε for ^{3}He along the critical isochore, and we find excellent consistency between the data of different series. The solid line and the dashed line are fits of the MC expression to the experiment with two different choices of the only free parameter, q_D, 3.0×10^6 cm^{-1} (solid line) and 5×10^6 cm^{-1} (dashed line), to show the sensitivity of the fit. Clearly, the lower value gives the best fit over the whole temperature range, and is determined to within $\pm 0.5 \times 10^6$ cm^{-1} from various fit trials. The uncertainty is greatest close to T_c, where the large density gradients make the measurements very sensitive to the geometry of the cell.

For the fit in Fig. 13, we have used the critical exponent $z_\eta = 0.054$ predicted by the MC theory. Using again $q_D = 3.0 \times 10^6$ cm^{-1}, we have tested

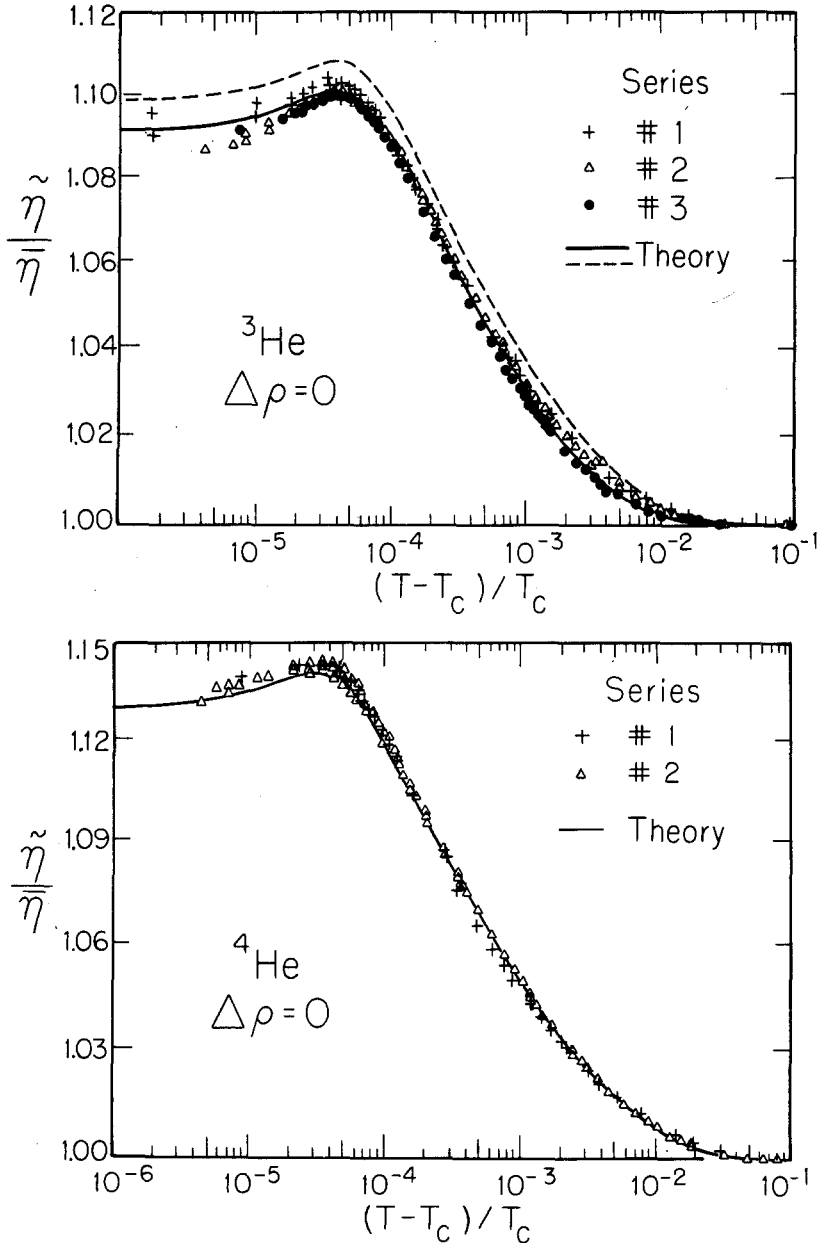Fig. 13. The measured normalized viscosity $\tilde{\eta}/\bar{\eta}$ versus ε along the critical isochore for (a) ^{3}He and (b) ^{4}He, indicated by symbols. (—) The best fits of the model calculation to the data with $q_D = 3 \times 10^6$ cm^{-1} for ^{3}He and 5×10^6 cm^{-1} for ^{4}He. (- -) The calculation for $q_D = 5 \times 10^6$ cm^{-1} for ^{3}He. A critical exponent $z_\eta = 0.054$ was used.

the sensitivity of the fit on the critical exponent value z_η. We found that, even though gravity effects prevent measurements from being carried out in the asymptotic "power law" regime, the fit is clearly sensitive to the critical exponent in the region above $\varepsilon = 10^{-4}$. A change of z_η from the value of 0.054 by ± 0.002 was found to cause the fit to deteriorate noticeably. This permits the conclusion that, within the framework of the MC expressions, $z_\eta = 0.054 \pm 0.002$, as determined from the quality of the fit given the estimated background viscosity $\bar\eta$.

In Fig. 13 we show a similar fit for ^{4}He with $z_\eta = 0.054$, leading to a parameter $q_D = 7 \times 10^6$ cm^{-1}, and just as for ^{3}He, the fit agrees with the data within the experimental scatter, except for the region dominated by gravity effects. The inverse value of q_D for both ^{3}He and ^{4}He is of the same order as the interatomic distances, a result that appears reasonable; however, it comes as a surprise that the values are different by a factor of more than 2 (the cubic root of the critical molar volume ratio for ^{4}He and ^{3}He is ~ 0.92). This difference might be due to the ambiguity in the estimation of $\bar\eta$ near T_c.

Figure 14 shows the normalized viscosity of ^{3}He along isotherms, where the data points shown were obtained from the various isochores at selected reduced temperatures where gravity effects are negligible; this is for $\varepsilon > 1.5 \times 10^{-4}$. The solid curves are calculated from the MC theory with the
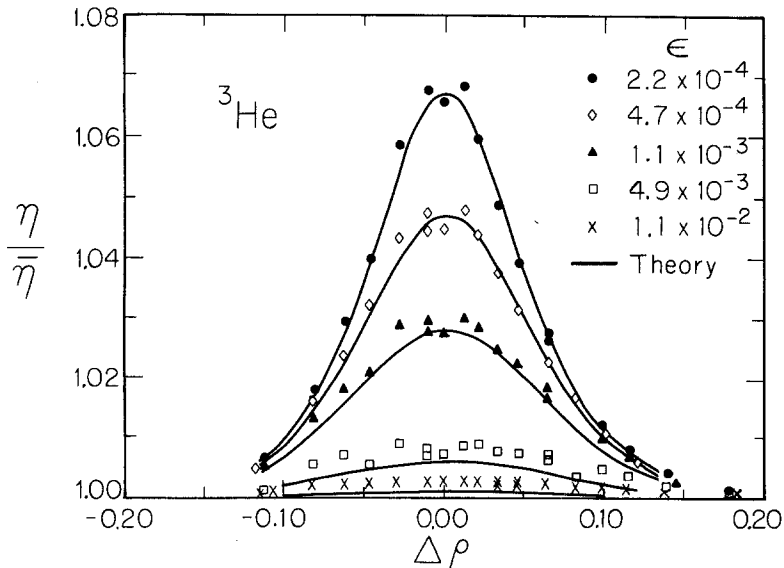

Fig. 14. The normalized viscosity $\bar\eta/\bar\eta$ for ^{3}He versus $\Delta\rho_c$ along several isotherms. (—) Fits of the MC theory with $q_D = 3 \times 10^6$ cm^{-1}.
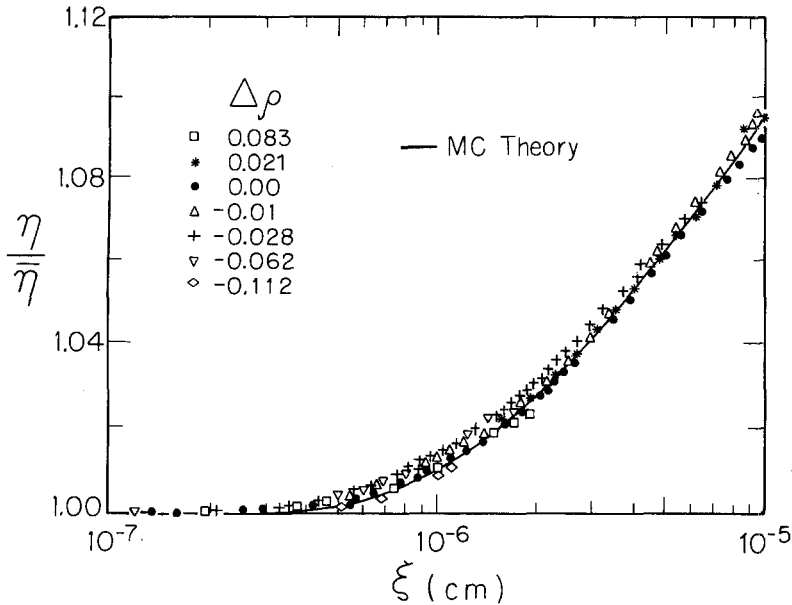
Fig. 15. Plot of $\eta/\bar{\eta}$ versus ξ for ^{3}He. The symbols indicate various isochores. (—) Calculated from the MC theory with $q_D = 3 \times 10^6$ cm^{-1}. Only data in the regions not affected by gravity are shown.

same input parameters as for Fig. 13 along the critical isochores. Again the agreement is excellent with $q_D = 3 \times 10^6$ cm^{-1}.

A more general plot is presented in Fig. 15, where it is shown that the normalized viscosity for ^{3}He for all the isochores approximately scales in ξ. To avoid overcrowding, only seven isochores are presented. The solid line is calculated from the MC theory with the same input parameters as before. Strictly speaking, the calculated curves for the various isochores do not exactly coincide, but in practice they differ by so little that they cannot be clearly distinguished on this plot.

In Fig. 16 we show a plot of $\eta/(\bar{\eta}\xi^{z_\eta})$ versus ξ^{-1} as suggested by Eq. (8), which includes the asymptotic and the first correction-to-scaling term. The temperature range chosen extends from about $\varepsilon = 1.5 \times 10^{-4}$ to 2×10^{-3}. The lower limit is set by the gradual development of the gravity effects, and the higher one by the condition that $\xi q_D > 1$ for the expansion. The error bars indicate the uncertainty of the critical temperature location, as discussed before, and this error becomes rapidly negligible as ξ^{-1} increases. If the exponent z_η is correctly chosen, this plot should produce a straight line of points. It can be seen that this is much more the case for $z_\eta = 0.054$ than for 0.065. Because there is some controversy[56] about the correctness of Eq.
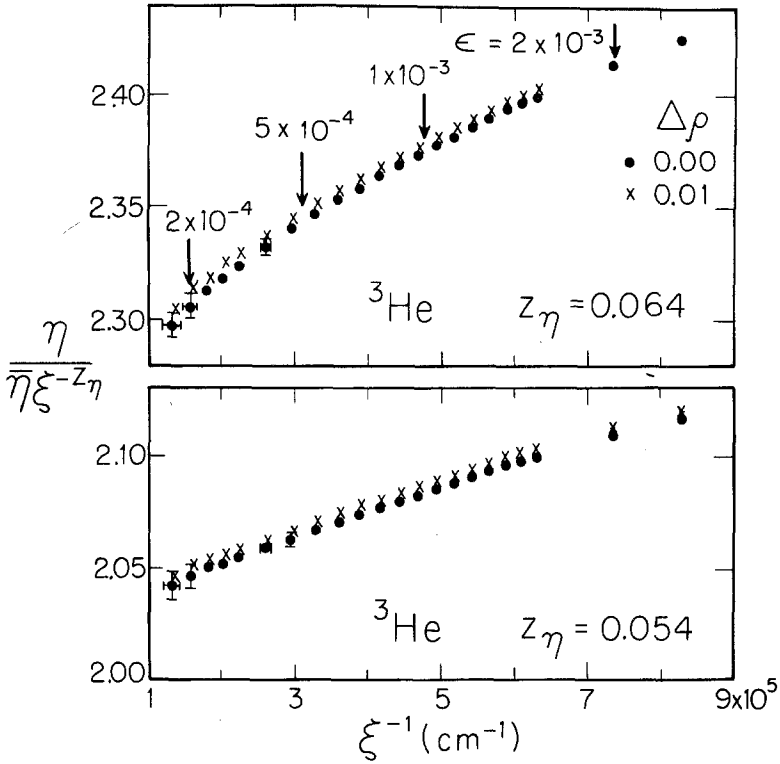
Fig. 16. Plot of $\tilde{\eta}/\bar{\eta}\xi^{z_\eta}$) versus ξ^{-1} for ^{3}He at two isochores very close to the critical one. The arrows indicate the corresponding reduced temperature ε. For $\varepsilon < 1.5 \times 10^{-4}$, gravity effects become noticeable. Top: $z_\eta = 0.064$. Bottom: $z_\eta = 0.054$.

(8), we have chosen the simple presentation of Fig. 16, rather than attempting a fit to determine the various parameters therein.

6.3. The Viscosity for He near the Coexistence Curve

Here we focus our attention on the viscosity's temperature dependence and on the position of its peak for near-critical isochores under the influence of gravity. As can be gathered from the model calculations, gravity effects become negligible for $|\Delta\rho| \gtrsim 0.06$. Here we want to test the internal consistency of our data along several isochores.

In Fig. 17 we show the data for ^{3}He and for ^{4}He along several isochores, together with the model calculations using the same value of q_D as in Section 5.2. We note the good agreement between experiment and model calculations. Considering that we do not actually sample the viscosity at the walls
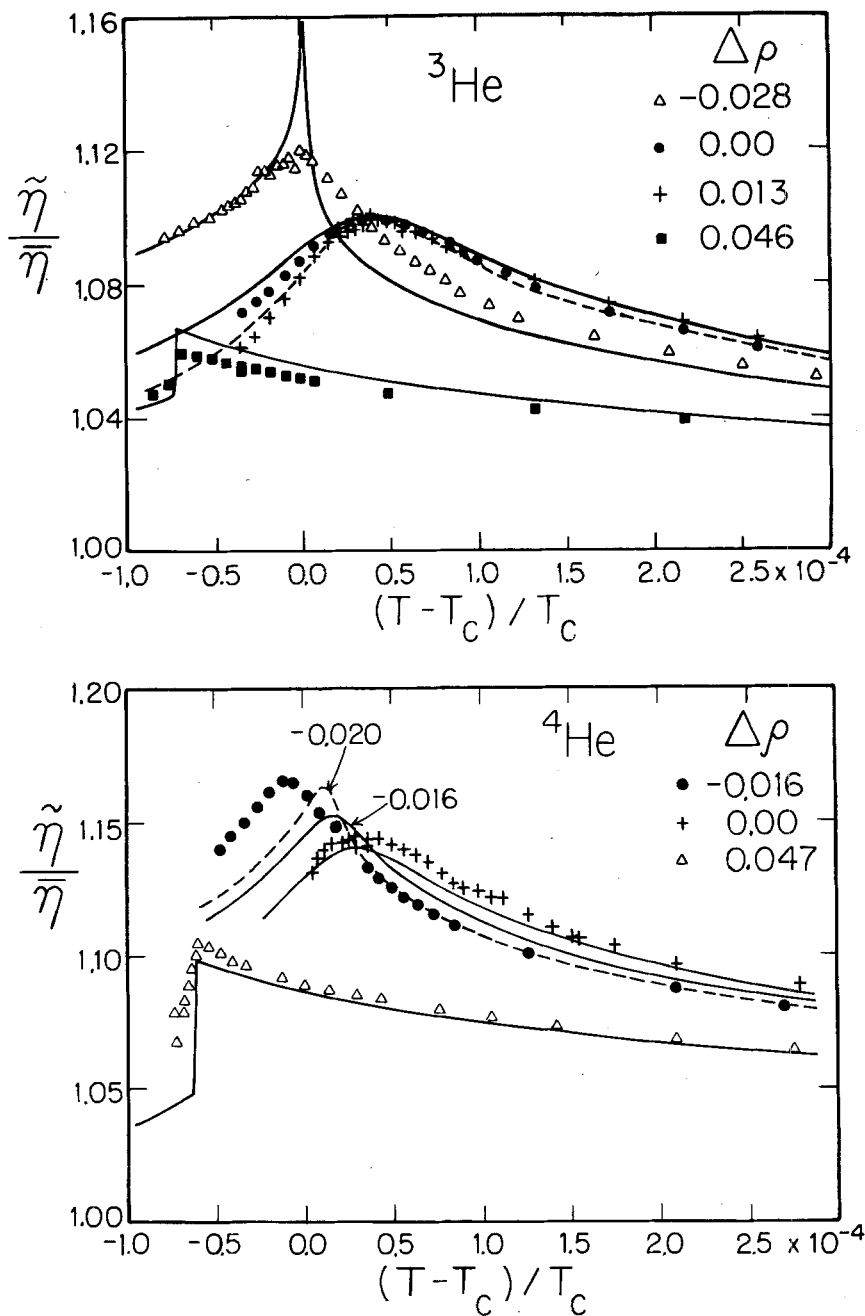
Fig. 17. The measured normalized viscosity $\tilde{\eta}/\bar{\eta}$ versus ε near the coexistence curve along several near-critical isochores for ^{3}He and ^{4}He, as shown by symbols, and compared with model calculations.
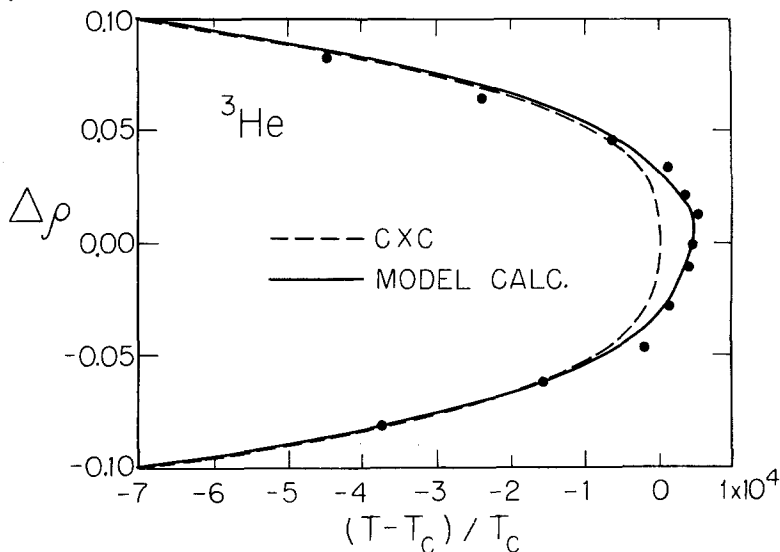
Fig. 18. The locus of the peaks or sharp changes in the observed viscosity near the coexistence curve of ^{3}He for a number of isochores. ($\bullet$) The data; (—) calculated from the model; (--) the coexistence curve.

of our viscometer as the model assumes, but in reality average over the penetration depth (see Figs. 7 and 8) in some nonlinear fashion, and considering furthermore the very different shapes of the $\tilde{\eta}$ variation versus ε along these isochores, the agreement is all the more remarkable. Although the critical viscosity $\eta/\bar{\eta}$ is symmetric with respect to ρ_c, gravity produces a density profile that is incorporated in the effective measured viscosity $\tilde{\eta}/\bar{\eta}$. The resulting asymmetry can be seen also in Fig. 18, where we plot for ^{3}He the η-peak position in temperature versus $\Delta\rho$ and compare it with the coexistence curve. Calculations show that the maximum peak temperature is at $\Delta\rho = 0.01$, which is consistent with the experiments. Again, there is good agreement between model calculations and the experiment. Similar calculations have been made for ^{4}He, where the density range was smaller than for ^{3}He, making the agreement less convincing.

6.4. The Critical Viscosity of CO_2

In view of the success in fitting the MC model to ^{3}He and ^{4}He for the viscosity along the critical isochore, we wondered whether similar data on other pure fluids near T_c could also be fitted with a similar free parameter q_D. The only such data along ρ_c with a scatter comparable to ours are those taken by Bruschi and Torzo[7] in CO_2. These authors used a rotating disk of
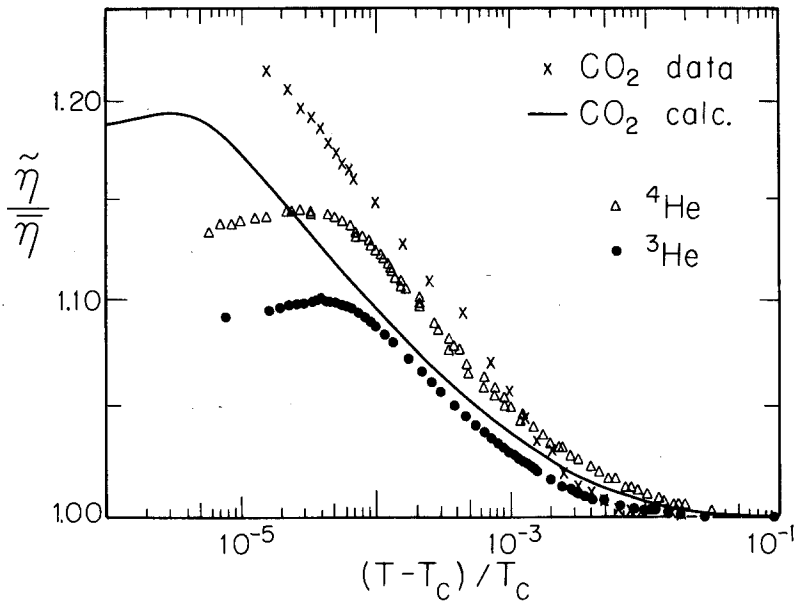
Fig. 19. The normalized viscosity $\eta/\bar{\eta}$ versus ε for CO_2 along the critical isochore. Symbols; Data by Bruschi and Torzo,[7] (—) Fit attempts of the theory including gravity effects calculation using $q_D = 1 \times 10^8$ cm^{-1} and $z_\eta = 0.054$. For comparison, the data for ^{3}He and ^{4}He along the critical isochore are shown.

0.2 mm thickness driven by magnetic induction and surrounded by the fluid, where T_c was located using critical opalescence.

The normalized data $\tilde{\eta}/\bar{\eta}$ taken from Fig. 2 of Ref. 7 are reproduced in Fig. 19 together with the model predictions using the parameters presented in Table I and $q_D = 1 \times 10^7$ cm^{-1}. The height separating the bottom and the top layers in contact with the disk was taken as 0.2 mm. These predictions are shown by a solid line, and two features are very different from our own helium data. First, CO_2 is affected much less by the gravity field than is helium, and thus the peak is shifted from T_c by only $\varepsilon = 3.5 \times 10^{-6}$. The smaller effect of gravity is consistent with criteria presented by Moldover et al.[21] The second difference is that the data cannot be fitted by the model, even by increasing q_D above 1×10^7 cm^{-1}, which produces very little change in the fit at such large values of q_D. Using an exponent z_η higher than 0.054 does not help either. Olchowy and Sengers[13] have independently discussed the CO_2 results[7] and found them inconsistent with other published CO_2 viscosity data along isotherms.

In Fig. 19, the viscosity data[7] for CO_2 are compared with those for ^{3}He and ^{4}He. We note that the singular behavior starts at a smaller ε than for

He ($\sim 9 \times 10^{-3}$ for CO_2 versus 5×10^{-2} for He), and the crossover region is much smaller for CO_2. A quasiasymptotic power-law behavior extends up to $\varepsilon \sim 3 \times 10^{-3}$, while for helium this behavior does not extend beyond $\varepsilon \sim 2 \times 10^{-4}$.

6.5. The Critical Thermal Conductivity of ^{3}He

Our success with fitting the helium viscosity data to the MC theory including gravity effects prompted us to reexamine the thermal conductivity data of Pittman et al.[12] for ^{3}He along the critical isochore. Our hope was that a similar fit with the same single free parameter q_D could be made, which would confirm the value found for the viscosity. To this end, we used the MC conductivity expression, presented in Appendix A, together with the gravity-induced density gradient through the cell (Appendix D), as for the viscosity calculations. Here, however, in contrast to the viscosity, the entire fluid layer in the cell contributes to the observed conductivity, and hence an integration of the thermal resistivity λ^{-1} through the height of the cell must be performed to give the effective average λ.

From the data of Pittman et al.[12] it is clear that above 4 K, $\bar{\lambda}$ is easily determined from measurements along isotherms, but below 4 K, there is already a singular contribution. The interpolation of data to yield $\bar{\lambda}(\rho_c)$ in the crossover regime $\varepsilon \lesssim 10^{-1}$ has an uncertainty that it is difficult to assess. In Fig. 20 we show the data for $\Delta\lambda$ along the critical isochore, and in Fig.
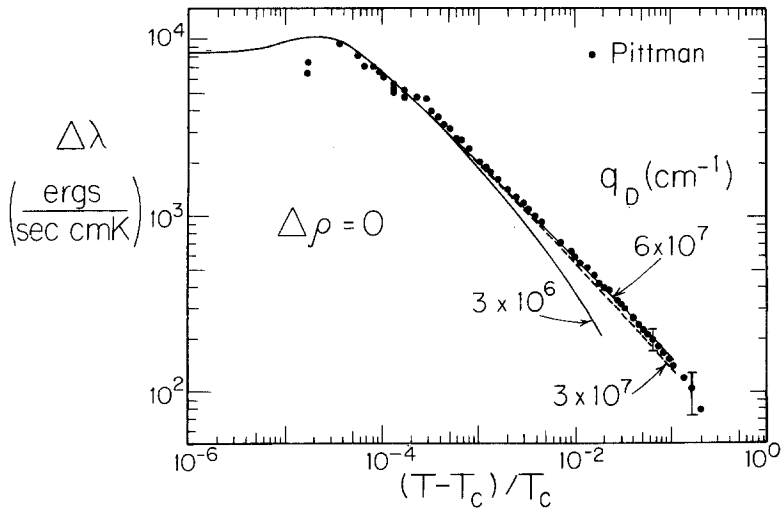

Fig. 20. The singular thermal conductivity $\Delta\lambda$ versus reduced temperature for ^{3}He along the critical isochore. ($\bullet$) Data by Pittman et al.[12] (—) MC model fit with $q_D = 6 \times 10^7$ cm^{-1}. (- -) Model fit with $q_D = 3 \times 10^7$ cm^{-1}.
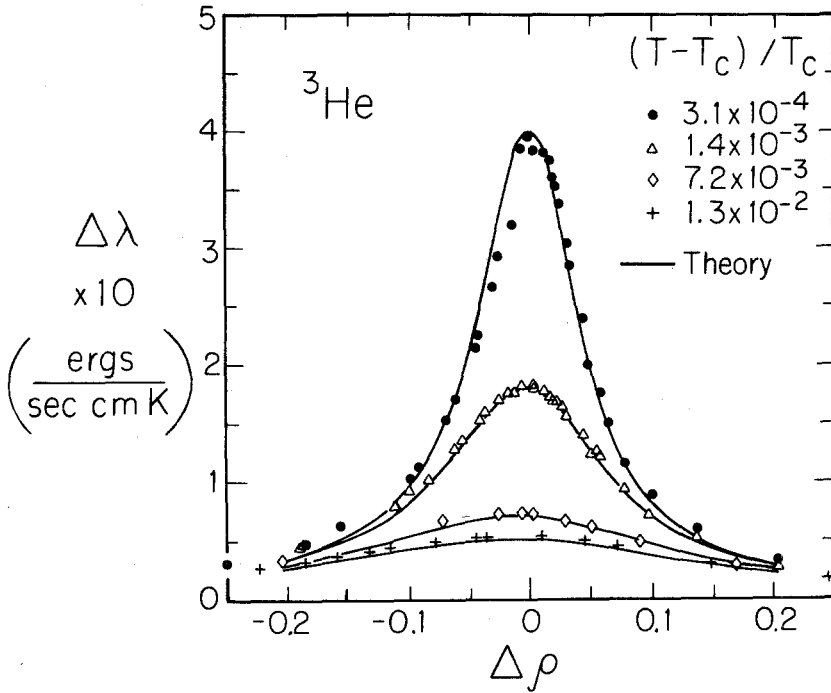
Fig. 21. The singular thermal conductivity $\Delta\lambda$ versus reduced density for several isotherms. Symbols; Data by Pittman *et al.*[12] (—) MC calculation with $q_D = 6 \times 10^7$ cm^{-1}.

21 along isotherms. The estimated uncertainty of $\Delta\lambda$ is indicated by error bars. Contrary to the presentation of the viscosity by means of a ratio $\eta/\bar{\eta}$, the critical conductivity is obtained by the subtraction $\lambda - \bar{\lambda}$, with a strongly increasing uncertainty as λ becomes nearly equal to $\bar{\lambda}$.

The singular term $\Delta\lambda$ was calculated from the MC theory using the same input parameters as for the viscosity calculation and using a calculated dependence of the viscosity on the density for the region where gravity effects become important. It was again apparent from the model that the conductivity peak would be located slightly above T_c at $\varepsilon_{\text{peak}} \approx 3.0 \times 10^{-5}$, in the same direction as for the viscosity. Accordingly, the temperature of the data was adjusted to situate the observed peak at the calculated value of $\varepsilon_{\text{peak}}$. The quality of the model calculation fit to the critical isochore data shown in Fig. 20 by the dashed and solid lines was acceptable for $q_D = (3–6) \times 10^7$ cm^{-1}. This value is 10–20 times larger than for the viscosity data. The solid curve for $q_D = 3 \times 10^6$ cm^{-1} (representing the fit value to viscosity data) is shown to demonstrate the dependence of the calculation on the value of q_D. For the isotherm data in Fig. 21 we only present the calculated

curves for $q_D = 6 \times 10^7$ cm^{-1}, which represent the data quite well. For $\varepsilon = 3.1 \times 10^{-4}$, the data points are somewhat asymmetric with respect to the critical density. We believe that this is caused by a systematic error in the density. Measurements of ρ were made[12] in a cell situated in close proximity to the thermal conductivity cell and in thermal contact with it. A capillary tube permitted fluid flow communication. If there was a slight temperature gradient ∇T between the two cells, there had to be a density gradient $\nabla \rho$ between them, proportional to $\alpha_T \nabla T$, where α_T is the isobaric thermal expansion coefficient (pressure gradients from gravity were calculated to have a negligible effect). Since α_T diverges at T_c, $\nabla \rho$ could become of the order of 1–2% for small enough ε and for densities near ρ_c.

The disappointing disagreement between the q_D obtained from viscosity and thermal conductivity measurements in ^{3}He prompted us to make an analysis of unpublished conductivity data[57] in ^{4}He along isotherms for $9.6 \times 10^{-3} \lesssim \varepsilon$. Just as for ^{3}He, the critical contribution $\Delta \lambda$ extends much further above T_c than for the viscosity. From Fig. 3 of Ref. 49, the existence of this contribution can be detected up to 8 K ($\varepsilon = 5.3 \times 10^{-1}$). A fit of the MC expressions[13] to several isotherms and also to $\Delta \lambda$ along the critical isochore, obtained by interpolation from isotherm data, results in a value of $q_D = (2–4) \times 10^7$ cm^{-1}, again well above that obtained from viscosity measurements, $q_D = 7 \times 10^6$ cm^{-1}.

In both the situations for ^{3}He and ^{4}He, a cutoff in the $\Delta \lambda$ tail at smaller ε would have produced a smaller q_D and hence a better agreement with the viscosity data analysis. Although there is little uncertainty about the data for the total conductivity, it is not excluded that separation into a "background" and a "singular" contribution is somewhat ambiguous. However, if $\Delta \lambda$ is calculated from MC theory with the q_D from the viscosity, this singular part vanishes for $\varepsilon \gtrsim 1 \times 10^{-1}$ (see Fig. 20). Then the isotherms above this temperature would represent "background" conductivity. Such isotherms are those for $T = 4.135$ K and above for ^{3}He (Fig. 7 in Ref. 12) and for $T = 6$ K and above for ^{4}He (Fig. 3 in Ref. 49). Clearly however, an anomalous contribution is still visible for these isotherms.

We note also the different way q_D affects the model calculations for η and $\Delta \lambda$, as already pointed out in Section 2. The conductivity in the asymptotic critical region is independent of q_D, while for the viscosity q_D affects the calculation over the whole temperature range. If q_D is shifted from its correct value, the whole curve is displaced, making the fit a poor one along its whole length. For these reasons, we feel that the q_D from η data is determined more sensitively than from the conductivity results but only $\bar{\eta}$ can be estimated correctly.

However, Sengers[56] believes that on the contrary the determination of q_D should be made from a fit to the thermal conductivity data. His reasons

are as follows: since q_D is the maximum wave number of the long-range fluctuations, the critical fluctuations should no longer contribute at temperatures and densities away from the critical point, where ξ becomes of the order of q_D^{-1}. Thus, q_D is related to the range of critical enhancement. Because of the mode coupling, this range is the same for the thermal conductivity and viscosity, but we have seen that in most of this range, the viscosity enhancement is small. Hence, Sengers feels that q_D should be determined from thermal conductivity data. A fit of the theory to the viscosity data will give q_D values that are sensitive to the approximations used, and will have less physical significance, he believes.

6.6. The Universal Dynamic Amplitude Ratio $\mathscr{R}$

The ratio $\mathscr{R}$, defined by Eq. (14), has been calculated for ^{3}He using the various properties along the critical isochore obtained as follows:

1. The viscosity η was obtained from the data presented in this paper and $\Delta\lambda$ from Ref. 12. As discussed before, the absolute value of η, normalized to the viscosity of ^{4}He at T_λ, is estimated to be known to $\pm 3\%$ or better, and that of $\Delta\lambda$ is $\pm 5\%$ when $\lambda \gg \bar\lambda$.

2. The specific heat ρC_p was calculated from measurements[9-11] of ρC_v, $(\partial P/\partial T)_\rho$, and β_T. We estimated the accuracy of ρC_p to be $\sim 5\%$.

3. The correlation length was taken from Table I.

The resultant ratio calculation was limited to the region $10^{-4} < \varepsilon < 10^{-2}$ because of gravity effects for small ε and the uncertainty of $\Delta\lambda$ at larger ε, when $\Delta\lambda \ll \lambda - \bar\lambda$. The results are shown in Fig. 22, where the error on each point, ± 0.1, includes the absolute estimated uncertainty of all terms in Eq. (14). Our average limiting value $\mathscr{R} = 1.05 \pm 0.1$ is found to be in good agreement with the predictions, $\mathscr{R} = 1.03$[28] and $\mathscr{R} \approx 1.04$.[23]

As was pointed out elsewhere,[29] the total thermal diffusivity $D_T = \lambda/\rho C_p$ from the conductivity and thermodynamic measurements is smaller by $\sim 15\%$ than D_T from light scattering data, which would lead to $\mathscr{R} \approx 1.2$. These last measurements, carried out at a small scattering angle θ, were very sensitive to a small systematic reading error in θ, which could partially at least account for the discrepancy. We place more weight on the determination of the singular part of D_T from the λ and the ρC_p data. There, the background value of $\lambda/\rho C_p$ was better determined than from light scattering experiments, which could not be carried out for $\varepsilon > 10^{-2}$ because of the low scattering intensity.

7. SUMMARY AND CONCLUSIONS

We have developed a torsional oscillator designed to measure the viscosity η of helium near the liquid–vapor critical point. This oscillator
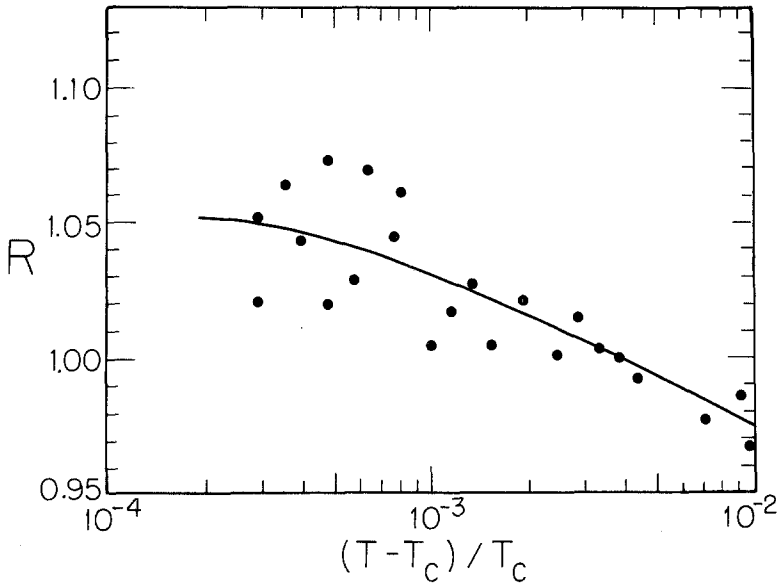
Fig. 22. The dynamic amplitude ratio $\mathscr{R}$ for ^{3}He calculated from various static and transport properties versus ε. On each point there is a systematic error of ± 0.1 reflecting the combined uncertainties in these properties.

operates at 158 Hz and is able to measure η with a precision of 0.05% and an absolute accuracy of $\sim 3\%$. Over the range of linear and stable operation, the calculated shear rate S covers the range $0.5 < S < 50 \sec^{-1}$.

We have carried out viscosity measurements on ^{3}He and ^{4}He along a number of critical isochores and over a large enough temperature range to permit a good determination of the background viscosity in addition to the singular one. The principal results of this research can be summarized as follows:

1. The temperature dependence of the background viscosity $\bar\eta$ is a sensitive function of the density, and $d\bar\eta/dT$ is quite different for ^{3}He and ^{4}He, for instance, along the critical isochores. A rough extrapolation of the data for ^{3}He to zero density near 3.35 K gives a value that is consistent with predictions. We note the ambiguity in determining $\bar\eta$ near T_c and its importance in the fit of η to critical dynamics theories.

2. Just as for the static properties, the apparent (measured) viscosity $\tilde\eta$ in helium is influenced strongly by the earth's gravitational field, which limits the viscosity singularity to 10% for ^{3}He and 14% for ^{4}He above $\bar\eta$.

3. Model calculations incorporating both the recently developed mode coupling theory expressions by Olchowy and Sengers and the vertical fluid density gradient in the cell from the earth's field can be fitted well to the

data along the critical isochore and the isotherms. The fit uses the experimental calorimetric and the equation-of-state data, expressed by the cubic model with coefficients and exponents tabulated by Sengers and Sengers, and the critical exponent $z_\eta = 0.054$. The fit then has only one free parameter, the cutoff wave number q_D. The inverse of the best fit values for q_D in ^{3}He and ^{4}He, $q_D = 3 \times 10^6$ and 7×10^6 cm^{-1}, is of the order of the interatomic distance, a reasonable result. The quality of the fit is quite sensitive to the value of z_η and is best for $z_\eta = 0.054$.

4. These model calculations have also been carried out to predict viscosity measurements near the coexistence curve for near-critical isochores. They show remarkable agreement with the experiments, which exhibit a peculiar behavior due to gravity effects.

5. A similar analysis has been carried out for the CO_2 data by Bruschi and Torzo along the critical isochore. However, a satisfactory fit could not be obtained.

6. Furthermore, model calculations using the theory for the singular thermal conductivity $\Delta\lambda$ in ^{3}He have been fitted to experiments in this laboratory, both along the critical isochore and along isotherms. The fit yielded $3 \times 10^7 < q_D < 6 \times 10^7$ cm^{-1} for ^{3}He, while ideally it should have been the same as for the viscosity. For ^{4}He, a fit of the MC expressions to conductivity data gives $2 \times 10^7 < q_D < 4 \times 10^7$ cm^{-1}, again higher than from the viscosity data analysis. The width of the range for q_D is determined by the uncertainty in the background conductivity subtraction. In spite of the unfortunate inconsistency, which remains to be clarified, one can state that q_D^{-1} is of the order of interatomic distances, a plausible result.

7. A plot of the viscosity to bring into evidence the asymptotic term and the first correction-to-scaling term from a series expansion in both the MC and the DRG theory again indicates the exponent $z_\eta = 0.054$ to be more correct for helium than $z_\eta = 0.065$.

8. Finally, using experimental data of η, $\Delta\lambda$, and static properties, we calculated the dynamic critical amplitude ratio $\mathcal{R}$ as a function of the reduced temperature along the critical isochore. As T_c was approached, the asymptotic limit was found to be $\mathcal{R} = 1.05 \pm 0.1$, in good agreement with predictions.

APPENDIX A. THE MC FORMULAS OF OLCHOWY AND SENGERS

In this Appendix, we will present expressions for the critical viscosity and the thermal conductivity derived by Olchowy and Sengers, which were used in the analysis of the data obtained in this laboratory.

The function H, defined in Eq. (3), which leads to the viscosity, is given by

$$H(q_D\xi, z, B)$$

$$= \left[\frac{\sin 3y_D}{12} - \frac{z}{4}\sin 2y_D + \left(z^2 - \frac{5}{4} - 2B\right)\sin y_D + z\left(\frac{3}{2} + 3B - z^2\right)y_D\right]$$

$$- \frac{(1+B)^2}{z}\left(\frac{B}{1+B}\right)^{1/2}\tan^{-1}\left[\left(\frac{B}{1+B}\right)^{1/2}q_D\xi\right]$$

$$+ [(1+3B)(1+B) - 2z^2 + z^4 - 4Bz^2]L_1(y_D)$$

$$+ \frac{B}{z}[(1+B)^2 - 2z^2 + z^4 - 3Bz^2]L_2(y_D)$$

where

$$y_D = \tan^{-1}(q_D\xi)$$

$$z = F/G$$

$$L_1(y_D) = \frac{1}{u-v}[uI(u, y_D) - vI(v, y_D)]$$

$$L_2(y_D) = \frac{1}{u-v}[I(v, y_D) - I(u, y_D)]$$

$$I(x, y) = \frac{1}{(1-x^2)^{1/2}}\ln\frac{1+x+(1-x^2)^{1/2}\tan(y/2)}{1+x-(1-x^2)^{1/2}\tan(y/2)}$$

$$u = \frac{z}{2}\left[1 + \left(1 - \frac{4B}{z^2}\right)^{1/2}\right], \qquad v = \frac{z}{2}\left[\left(1 - \frac{4B}{z^2}\right)^{1/2}\right]$$

The definitions for B, G, and F are given in Eq. (4).

For the calculation of the thermal conductivity $\Delta\lambda$, the expression defined in Eq. (13) is given by

$$\Omega(q_D\xi, B)$$

$$= \frac{1}{1+B}\frac{2}{\pi}\mathcal{R}\left[\tan^{-1}(q_D\xi) + \frac{B}{G}\ln\left(\frac{1+\sin y_D}{1-\sin y_D}\right)^{1/2}\right.$$

$$+ \left.\sum_{i=1}^{3} A_i(z_k, G, F, B)I(z_i, y_D)\right]$$

$$- \frac{2}{\pi}[1 + Gy_D + F(1+B)^{-1}]\left[1 - \exp\left(\frac{-q_D\xi}{1+(q_D\xi)^3\rho_c^2/3\rho^2}\right)\right]$$

where

$$A_i = \frac{Fz_i - (B/G)(G^2 + B + F) - (z_i^2/G)(G^2 + B)}{\prod_{k\neq i}(z_i - z_k)}$$

$$z_1 = \tfrac{1}{3}G + (s_1 + s_2)$$

$$z_2 = \tfrac{1}{3}G - \tfrac{1}{2}(s_1 + s_2) + \tfrac{1}{2}j \cdot 3^{1/2}(s_1 - s_2)$$

$$z_3 = \tfrac{1}{3}G - \tfrac{1}{2}(s_1 + s_2) - \tfrac{1}{2}j \cdot 3^{1/2}(s_1 - s_2)$$

$$\begin{matrix} s_1 \\ s_2 \end{matrix} = [\, r \pm (s^3 + r^2)^{1/2}\,]^{1/3}$$

$$r = B^{*3/2} \varepsilon^{*1/2}(\Delta^*/2 - 1/6 + \varepsilon^*/27)$$

$$s = \tfrac{1}{3}B^*(1 - \tfrac{1}{3}\varepsilon^*)$$

$$\varepsilon^* = G^2/(B+F); \qquad \Delta^* = B/(B+F); \qquad B^* = B + F$$

$$j = (-1)^{1/2}$$

APPENDIX B. THE COMPRESSIBILITY OF ^{3}He ALONG THE CRITICAL ISOCHORE

In order to check the reduced temperature range over which the compressibility β_T along ρ_c could be represented by a simple power law, we have extended previous data[11] of ^{3}He up to a temperature of 11 K ($\varepsilon \simeq 2.5$) by measuring the density versus pressure along 15 isotherms. The resulting compressibility along the critical isochore is presented in Fig. 23, together with the extrapolated curve from the data by Pittman et al.,[11] with
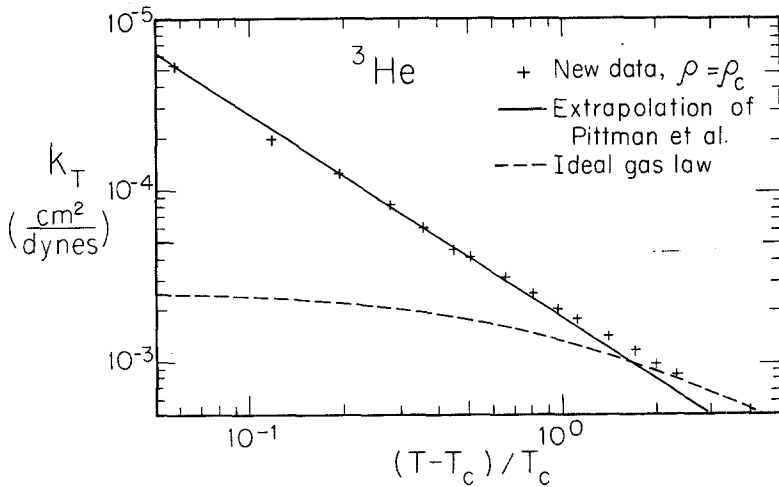

Fig. 23. The isothermal compressibility for ^{3}He along the critical isochore. ($\times$) New data. (—) Power law from the data by Pittman et al.[11] extrapolated beyond $\varepsilon = 6 \times 10^{-2}$. (- -) Compressibility of an ideal gas.

$\gamma_{\text{eff}} = 1.20$. Within the experimental scatter, the new data follow the simple power law up to $\varepsilon \simeq 0.5$. Further from T_c, the compressibility approaches the curve $(RT)^{-1}$ for an ideal gas, as shown by the dashed curve. Such a "background" estimation is no doubt oversimplified because of the expected departure of ^{3}He from an ideal behavior at low temperatures, but at least it gives a value that at 8 K is not too far from the experimental value of k_T. We have also calculated the compressibility of ^{3}He using the second virial expansion computed by Kilpatrick et al.[58] and found the predicted k_T to lie appreciably above the data. Thus, the second virial expansion does not provide a good expression for the background compressibility.

APPENDIX C. HYDRODYNAMIC EQUATIONS FOR THE FLUID PERTURBED BY OSCILLATING DISKS

Here we present the equations leading to the relation between the viscosity and the experimental parameters in the torsional oscillator measurement. This presentation follows to a great extent that in Shaumeyer's thesis.[33]

Consider a fluid layer of height h between two horizontal circular plates of radius R, such that $R \gg h$. Define the vertical coordinate z, where $z = 0$ in the middle between the plates, so the upper and lower plates are located at $z = \pm h/2$. Also define a horizontal coordinate r with its zero at the disk center, and define an angle of rotation θ around the axis with respect to a fixed coordinate system.

The disks are made to oscillate in phase with an amplitude $\theta = \theta_0 e^{i\omega t}$, which is assumed to be small enough that the motion of the fluid is harmonic. The fluid displacement $u(r, \theta, z, t)$ is assumed to be only in the direction of θ, and we also assume cylindrically symmetric fluid motions, $\mathbf{u} = \hat{\theta} u_\theta$ with $\partial u_\theta / \partial \theta = \partial^2 u_\theta / \partial \theta^2 = 0$. Given these assumptions, and setting $u_\theta = r\Omega(z, t)$, one finds the Navier–Stokes equation in cylindrical coordinates reduced to

$$\frac{\partial \Omega}{\partial t} = \frac{\eta}{\rho} \frac{\partial^2 \Omega}{\partial z^2} \tag{C.1}$$

We first consider the case of $R \to \infty$. When we apply the boundary condition that the fluid at the walls $(z = \pm d/2)$ is locked to the disks, the solution of this equation for a simple harmonic motion becomes

$$\Omega(z, t) = \frac{\cos(kz)}{\cos(kd/2)} \dot{\theta}(t) \tag{C.2}$$

where

$$k = \pm(1 + i)(\rho\omega/2\eta)^{1/2} \tag{C.3}$$

Here we define the penetration depth

$$\delta = (2\eta/\rho\omega)^{1/2} \tag{C.4}$$

the distance over which the amplitude of the shear wave falls off by a factor of e.

To calculate the torque Γ_f produced by the fluid on the walls of the container, we consider the frictional force $\sigma_{\theta,z}$ per area at any point on the boundary. We obtain

$$\sigma_{\theta,z} = \frac{E}{A} = -\eta\left(\frac{\partial u_\theta}{\partial z}\right)_{z=\pm d/2} = \eta k r \tan(kd/2) \cdot \dot\theta \tag{C.5}$$

The torque is then

$$\Gamma_f = \int r\sigma_{\theta,z}\, dA \tag{C6}$$

where the integration is over the disk surfaces of radius R. One then obtains

$$\Gamma_f = \pi\eta k R^4 \tan(kd/2) \cdot \dot\theta(t) \tag{C.7}$$

Here k is still a complex quantity. It can be shown, however, that if the ratio $h/2\delta$ is much greater than unity (which is realized in our viscometer geometry), then $\tan(kd/2) \simeq i$ and the torque can be written as

$$\Gamma_f = (i-1)\dot\theta(t)2\omega I_f \tag{C.8}$$

where

$$I_f = \frac{\pi}{2}\rho\frac{\lambda}{2}R^2 \qquad \text{(disks)} \tag{C.9}$$

which is the moment of inertia of a layer of fluid one-half the penetration depth thick.

Shaumeyer and Behringer[33] have also treated the fluid motion inside an oscillating cylinder of radius R and infinite height. They calculated the torque due to a section h of this cylinder, with $h \gg \delta$. The equation for the torque can then be expressed again by Eq. (C.8), but with

$$I_f = \pi\rho\frac{\lambda}{2}R^3 h \qquad \text{(cylinder)} \tag{C.9a}$$

Thus, for our geometry, including friction on the horizontal disks and on the vertical walls, but ignoring small corner effects, the total effective moment of inertia of the fluid is

$$I_f = \frac{\pi}{2}\rho\frac{\lambda}{2}R^3(R+2h) \tag{C.9b}$$

In our specific case, the vertical wall contribution represents a 3% additive correction.

The equation of motion of the torsional oscillator filled with fluid is now

$$I_s\ddot{\theta}(t) = -K\theta + \Gamma_D + \Gamma_F + \Gamma_E \tag{C.10}$$

where I_s is the moment of inertia of the container, $\Gamma_D = De^{-i\omega t}e^{i\Phi}$ is the driving torque with an arbitrary constant phase Φ and real amplitude D, $\Gamma_E = \omega E\dot{\theta}(t)$ is the empty-cell damping term, and $-K\theta$ is the elastic restoring torque of the fiber.

Inserting a solution $\theta = \theta_0 e^{-i\omega t}$ into Eq. (C.10), we obtain

$$(D/\theta_0)\, e^{i\Phi} = [K - \omega^2(I_s + I_f)] - i[\omega^2(I_f + E)] \tag{C.11}$$

The inverse response function $G^* \equiv (D/\theta_0)^2$ can be obtained by taking the absolute value of both sides of (C.11) and defining $I = I_s + I_f$ as the total inertial term and $F \equiv I_f + E$ as the total dissipative term. One then obtains

$$G^* = (K - \omega^2 I)^2 + \omega^4 F^2 \tag{C.12}$$

The inverse response function G^* should be at a minimum when the oscillator is at resonance at a frequency ω_r. In the situation where $I \gg I_f$, the resonant frequency is given by

$$\omega_r^2 = KI/(I^2 - F^2) \simeq K/I \tag{C.13}$$

Using Eq. (C.11), we find

$$\tan \Phi = -\omega^2 F/(K - \omega^2 I) \tag{C.14}$$

where it can be seen from Eq. (C.13) that Φ will be nearly 90° at resonance.

For freely decaying oscillations, we have $D = 0$. Inserting the oscillator motion equation $\theta = \theta_0 \exp[-t(i\omega - \tau^{-1})]$ into Eq. (C.10) and equating the real and imaginary parts, one obtains

$$(-\omega^2 + \tau^{-2})I_s = -K - \omega F(\omega + \tau^{-1}) \tag{C.15}$$

$$\omega = (F - 2I_s)/F\tau \tag{C.16}$$

Inserting Eq. (C.16) into Eq. (C.15), one obtains

$$\tau^2 = -\frac{1}{K}\frac{2F^3 - 6F^2 I_s + 4FI_s^2 - 4I_s^3}{F^2} \tag{C.17}$$

and finally

$$\tau \simeq \frac{2I_s}{F}\left(\frac{I_s}{K}\right)^{1/2} = \frac{2Q_T}{\omega_r} \tag{C.18}$$

where $Q_T \simeq I_s/F$ is the quality factor of the total system.

APPENDIX D. THE EARTH'S GRAVITY EFFECTS

Here we outline the method used to calculate the vertical profile of the density in the cell $\rho(z)$ due to gravity and deduce the corresponding correlation length $\xi(z, \varepsilon)$. Calculation of $\rho(z)$ already has been presented by Hohenberg and Barmatz[51] using the linear model equation of state. We have carried out similar calculations using the cubic model.[20]

The method for using this model consists in picking a temperature and an average density, finding the height of the critical density ρ_c, and then using the change in the chemical potential $d\mu = -g\,dz$, where g is the gravitational acceleration, to calculate the density as one moves above or below the critical density. The vertical density profile is not dependent on the cell height h per se, but on ε and on the distance in the vertical direction from the level of ρ_c even if ρ_c is predicted to fall outside the cell.

We use the cubic model relations

$$\mu(\rho, T) - \mu(\rho_c, T) = (P_c/\rho_c)a\theta(1 - \theta^2)r^{\beta\delta} \tag{D.1}$$

$$\varepsilon = (1 - b^2\theta^2)r \tag{D.2}$$

$$\Delta\rho \equiv (\rho - \rho_c)/\rho_c = k(1 + c\theta^2)\theta r^{\beta} \tag{D.3}$$

where a and k are fluid-dependent constants, $b^2 = 3(3 - 2\beta)^{-1}$, $c = (\beta\delta - 3)(3 - 2\beta)^{-1}$, and r and θ are the parameters. We then make the choice that ρ_c (or the meniscus) is always at a height $z^* = 0$ and we find

$$z^* = C\theta(1 - \theta^2)r^{\beta\delta} \tag{D.4}$$

$$C = -aP_c(\rho_c gh)^{-1} \tag{D.5}$$

Here z^* is expressed in units of h. Solving the parametric equations (D.1)–(D.5) will yield $\rho(z^*)$. In order to find the locus of the critical density with respect to the cell bottom, z_1^*, one needs to find the zero value of the function

$$F(z_1^*) = \bar{\rho} - \int_{z_1^*}^{z_1^*+1} \rho(z^*)\,dz^* \tag{D.6}$$

Here $\rho(z^*)$ is known as a function of θ, and the integrand then reads

$$\rho(z^*)\,dz^* = -\varepsilon^{-1}\rho(\theta)Cr^{1+\beta\delta}\{1 + [(2\beta\delta - 1)b^2 - 3]\theta^2 + b^2(3 - 2\beta\delta)\theta^4\}\,d\theta \tag{D.7}$$

Both the parametric equations and the zero of $F(z_1^*)$ were solved by computer using a bisection root finder, in preference to Newton's method, which was often found to be unreliable very near the critical point. The coordinate change $z = (z^* - z_1^* - 1/2)h$ gives consistency with the height z in Appendix C, where $z = 0$ is located in the middle of the fluid layer of height h.

The result from these equations made available θ and r at any height z in the container at a given ε and $\bar{\rho}$. Then the correlation length ξ could be obtained from the cubic model relation

$$\xi(\varepsilon, \Delta\rho) = \xi_0 r^{-\nu}(1 + 0.16\theta^2) \tag{D.8}$$

The value of $\xi(\varepsilon, \Delta\rho)$ in turn yielded the viscosity $\eta/\bar{\eta}$. And the singular thermal conductivity $\Delta\lambda$.

ACKNOWLEDGMENTS

REFERENCES

1. J. V. Sengers, *Int. J. Thermophys.* **6**, 203 (1985), and references therein.
2. K. Kawasaki, in *Phase Transitions and Critical Phenomena*, C. Domb and M. S. Green, eds. (Academic Press, New York, 1976).
3. P. C. Hohenberg and B. I. Halperin, *Rev. Mod. Phys.* **49**, 435 (1977).
4. D. Beysens, A. Bourgou, and G. Paladin, *Phys. Rev. A* **30**, 2686 (1984).
5. R. Berg and M. R. Moldover, to be published.
6. H. J. Strumpf, A. F. Collings, and C. J. Pings, *J. Chem. Phys.* **60**, 3109 (1974).
7. L. Bruschi and G. Torzo, *Phys. Lett.* **98A**, 265 (1983).
8. J. M. Goodwin, A. Hirai, T. Mizusaki, K. Tsuboi, and T. K. Waldschmidt, *Physica* **107B**, 351 (1981); J. M. Goodwin, private communication.
9. R. P. Behringer, T. Doiron, and H. Meyer, *J. Low Temp. Phys.* **24**, 315 (1976); B. Wallace and H. Meyer, *Phys. Rev.* **2A**, 1563 (1970).
10. G. R. Brown and H. Meyer, *Phys. Rev. A* **6**, 364 (1972).
11. C. Pittman, T. Doiron, and H. Meyer, *Phys. Rev. B* **20**, 3678 (1979).
12. C. Pittman, L. H. Cohen, and H. Meyer, *J. Low Temp. Phys.* **46**, 115 (1982).
13. G. Olchowy and J. V. Sengers, Technical Report BN 1052, Institute of Physical Science and Technology, University of Maryland, College Park, Maryland (1986), and private communication.
14. J. K. Bhattacharjee and R. A. Ferrell, *Phys. Rev. A* **27**, 1544 (1983).
15. M. E. Fisher, *Rev. Mod. Phys.* **46**, 597 (1974).
16. P. C. Hohenberg, *Physica (Utrecht)* **109–110B**, 1436 (1982).
17. V. Dohm and R. Folk, in *Advances in Solid State Physics*, Vol. 22, P. Grosse, ed. (Vieweg, Braunschweig, 1982), p. 1.
18. J. K. Bhattacharjee, R. A. Ferrell, R. S. Basu, and J. V. Sengers, *Phys. Rev. A* **24**, 1469 (1981).
19. R. A. Ferrell, *Phys. Rev. Lett.* **24**, 1169 (1970).
20. J. v. Sengers and J. M. H. Levelt Sengers, in *Progress in Liquid Physics*, C. A. Croxton, ed. (Wiley, Chichester, 1978), p. 103.

21. M. R. Moldover, J. V. Sengers, R. W. Gammon, and J. R. Hocken, *Rev. Mod. Phys.* **51**, 79 (1979), and references therein.
22. E. D. Siggia, B. J. Halperin, and P. C. Hohenberg, *Phys. Rev. B* **13**, 2110 (1976).
23. G. Paladin and L. Peliti, *J. Phys. Lett.* (Paris) **43**, L15 (1982); Erratum **45**, L299 (1984).
24. J. K. Bhattacharjee and R. A. Ferrell, *Phys. Rev. A* **28**, 2363 (1983).
25. R. Perl and R. A. Ferrell, *Phys. Rev. A* **6**, 2358 (1972).
26. J. K. Bhattacharjee and R. A. Ferrell, *Phys. Rev. A* **24**, 1643 (1981).
27. G. Arcovito, C. Faloci, M. Roberti, and L. Mistura, *Phys. Rev. Lett.* **22**, 1040 (1969).
28. H. C. Burstyn, J. V. Sengers, J. K. Bhattacharjee, and R. A. Ferrell, *Phys. Rev. A* **28**, 1567 (1983).
29. Y. Miura, H. Meyer, and A. Ikushima, *J. Low Temp. Phys.* **55**, 247 (1984).
30. E. Berthold, R. W. Giannetta, E. N. Smith, and J. D. Reppy, *Phys. Rev. Lett.* **37**, 1138 (1976).
31. R. Biskeborn and R. W. Guernsey, *Phys. Rev. Lett.* **34**, 455 (1975).
32. J. Parpia, Ph.D. Thesis, Cornell University (1980).
33. J. Shaumeyer, Ph.D. Thesis, Duke University (1984); J. Shaumeyer and R. P. Behringer, *Phys. Rev. B* **33**, 3553 (1986), and to be published.
34. P. Horowitz and W. Hill, *The Art of Electronics* (Cambridge University Press, Cambridge, 1980).
35. C. Agosta, Ph.D. Thesis, Duke University (1986).
36. E. C. Kerr and R. H. Sherman, *J. Low Temp. Phys.* **3**, 451 (1970).
37. H. A. Kierstead, *Phys. Rev. A* **7**, 242 (1973).
38. D. Dahl and M. R. Moldover, *Phys. Rev. A* **6**, 1915 (1972).
39. L. D. Landau and E. M. Lifshitz, *Fluid Mechanics* (Pergamon Press, London, 1959).
40. R. P. Reed and R. P. Miksell, *Low Temperature Mechanical Properties of Copper and Selected Alloys* (National Bureau of Standards Monograph 101, 1967).
41. G. Ahlers, in *Physics of Liquid and Solid Helium*, Part I, K. H. Bennemann and J. B. Ketterson, eds. (Wiley, New York, 1976).
42. L. Bruschi, G. Mazzi, M. Santini, and G. Torzo, *J. Low Temp. Phys.* **29**, 63 (1977).
43. R. W. H. Webeler and G. Allen, *Phys. Rev. A* **5**, 1820 (1972).
44. A. Michels, B. Blaisse, and C. Michels, *Proc. R. Soc. A* **160**, 358 (1937).
45. J. V. Sengers and J. M. J. Van Leeuwen, *Physica* **116A**, 345, (1982).
46. D. B. Roe and H. Meyer, *J. Low Temp. Phys.* **30**, 91 (1978).
47. M. R. Moldover, *Phys. Rev.* **182**, 342 (1969).
48. J. A. Lipa, C. Edwards, and M. J. Buckingham, *Phys. Rev. A* **15**, 778 (1977).
49. A. Acton and K. Kellner, *Physica* **90B**, 192 (1977).
50. A. Michels, J. V. Sengers, and P. S. Van der Gulik, *Physica* **28**, 1201, 1216 (1962).
51. P. C. Hohenberg and M. Barmatz, *Phys. Rev. A* **6**, 289 (1972).
52. J. A. Lipa, C. Edwards, and M. J. Buckingham, *Phys. Rev. Lett.* **25**, 1086 (1970).
53. J. De Boer, *Physica* **10**, 348 (1943).
54. J. De Boer and G. D. Cohen, *Physica* **27**, 993 (1951).
55. S. Wang and H. Meyer, to be published.
56. J. V. Sengers, private communication.
57. A. Acton and K. Kellner, private communication (1978).
58. J. E. Kilpatrick, W. E. Keller, E. F. Hammel, and N. Metropolis, *Phys. Rev.* **94**, 1103 (1954).